AD-A137 488 THE EFFECTS OF SUBSTRATE SURFACE TREATMENTS ON THE DEFECT INCORPORATION I..(U) COLORADO STATEUUIIV FORT COLLINS DEPT OF ELECTRICAL ENGINEERI.. 05 JAN 84 1/1

UNCLASSIFIED N00019-83-C-0034 F/G 20/12 NL

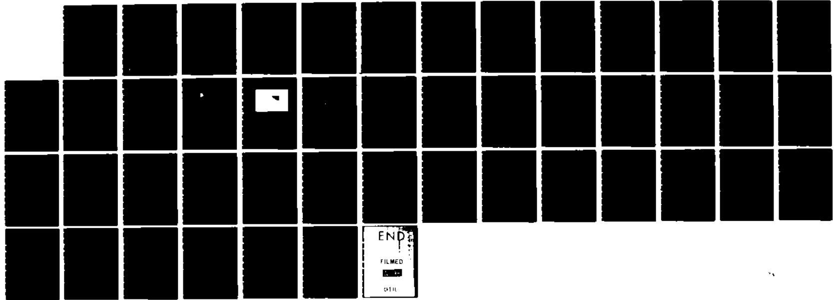

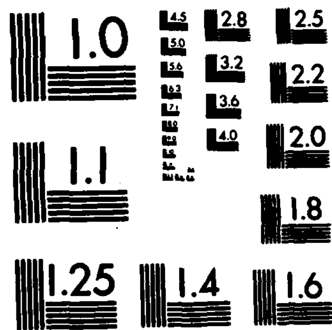
1.0
1.1
1.25
1.4
1.6
1.8
2.0
2.2
2.5
2.8
3.2
3.6
4.0
4.5
5.0
5.6
6.3
MICROCOPY RESOLUTION TEST CHART
NATIONAL BUREAU OF STANDARDS-1963-A

AD A137488

THE EFFECTS OF SUBSTRATE SURFACE TREATMENTS ON THE DEFECT INCORPORATION IN HYDRIDE VPE GROWN InGaAs FILMS

Final Report

January 6, 1983 - January 5, 1984

For

Naval Air Systems Command

Contract No. N00019-83-C-0034

DTIC
ELECTE
FEB 3 1984
A

Electrical Engineering Department

Colorado State University

Fort Collins, CO 80523

DTIC FILE COPY

84 02 03 067

APPROVED FOR PUBLIC RELEASE
DISTRIBUTION UNLIMITED

TABLE OF CONTENTS

Page

ABSTRACT-- 1

I INTRODUCTION-------------------------------------- 2
A. Surface and Interface Studies---------------------- 2
B. Growth Studies------------------------------------- 9

II EXPERIMENTAL PROCEDURE---------------------------- 11
A. Interface and Surface Studies---------------------- 11
B. Growth Studies------------------------------------- 22

III DISCUSSION--------------------------------------- 35
A. Interface and Surface Studies---------------------- 35
B. Growth Studies------------------------------------- 35

REFERENCES-- 40

LIST OF FIGURES

1. a.) The band diagram and charge distribution for the steady state. b.) The charge distribution when the electron traps have been filled by a zero biasing pulse. c.) The charge distribution when the hole traps have been filled by an optical pulse------------------------------------ 4

2. a.) The steady state and zero bias charge distribution a.) at a low temperature when $E_{tn} - (E_g - E_{Fn}) > q\phi_s$, b.) when $E_g - E_{Fn}$ is almost equal to E_{tn}, and c.) when $E_g - E_{Fn} > E_{tn}$-- 7

3. Surface of an InP film bathed a.) in PH_3 with one half of the surface covered (300x) and b.) in HCl (37.5x)---------- 12

4. InP films grown on a substrate bathed in PH_3 (left) and b.) a substrate etched in HCl (right)------------------- 13

5. InP films grown for HCl/PH_3 ratios of a.) 4.0/1.5 (37.5x) and b.) 1.0/2.0 (37.5x)-------------------------------- 14

6. The FET structure and a schematic of the electronics used in the current DLTS measurements----------------------------- 16

7. The square of the reciprocal of the capacitance plotted as a function of the reverse bias for a GaAs film grown on an InP substrate-- 18

8. The channel resistance plotted as a function of the reverse bias for a GaAs film grown on an InP substrate-------- 19

APPROVED FOR PUBLIC RELEASE
DISTRIBUTION UNLIMITED

LIST OF FIGURES--CONTINUED

		Page
9.	The log of the channel resistance plotted as a function of the reciprocal temperature for a GaAs film grown on an InP substrate	20
10.	The log of the change in the channel resistance plotted as a function of the time for T = -136 and 26°C for a GaAs film grown on an InP substrate	21
11.	The film growth rate plotted as a function of the input HCl pressure, HCl^o, when the partial pressures of PH_3 = .01 atm. and downstream HCl = 0	24
12.	The film growth rate plotted as a function of the input HCl pressure, HCl^o when the partial pressures of PH_3 = .015 atm. and downstream HCl = 0	25
13.	The film growth rate plotted as a function of the input HCl pressure, HCl^o, when the partial pressures of PH_3 = .01 atm. and the downstream HCl = .1 P_{HCl^o}	26
14.	The film growth rate plotted as a function of the PH_3 partial pressure when P_{HCl^o} = .007 atm. and there is no downstream HCl	27
15.	The film growth rate plotted as a function of the downstream HCl pressure, P_{HCl^2}, when P_{HCl^o} = .007 atm. and P_{PH_3} = .01 atm	28
16.	The film growth rate plotted as a function of the H_2 flow rate, when the HCl^o, HCl^2, and PH_3 flow rates are held constant	29
17.	The carrier concentration and the room temperature and LN mobilities plotted as a function of the input HCl concentration	31
18.	The carrier concentration and the room temperature and LN mobilities plotted as a function of the H_2 flow rate	32
19.	The system used to generate high purity HCl from PCl_3 or $AsCl_3$ or to provide PCl_3 or $AsCl_3$ for chloride growth	33
20.	Liquid nitrogen mobilities for InP plotted as a function of the carrier concentration	39

APPROVED FOR PUBLIC RELEASE
DISTRIBUTION UNLIMITED

LIST OF TABLES

Page

1. Initial results for room temperature and 77K carrier concentrations and mobilities for HCl from a cylinder and formed by cracking PCl_3---------------------------------- 34

2. Initial results for room temperature and 77K carrier concentrations and mobilities when the substrate is not etched and is etched in situ prior to deposition---------- 34

ABSTRACT

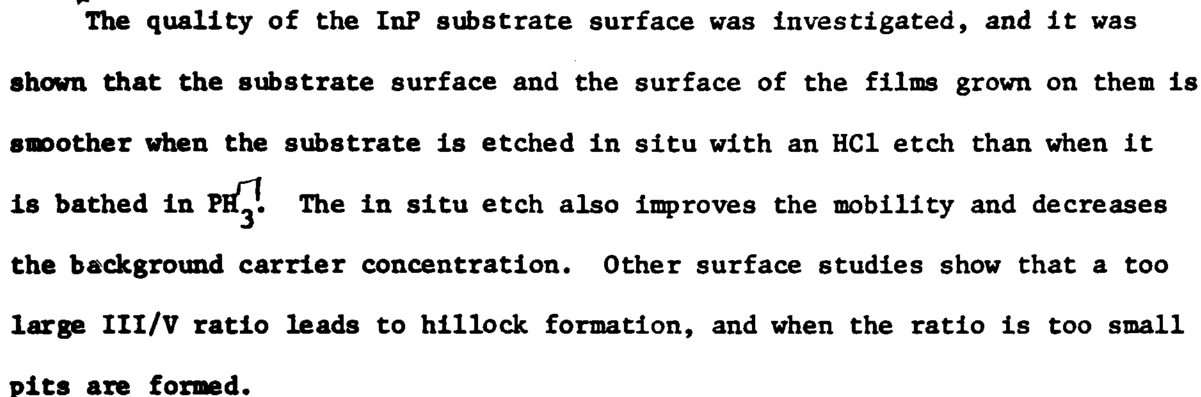

The quality of the InP substrate surface was investigated, and it was shown that the substrate surface and the surface of the films grown on them is smoother when the substrate is etched in situ with an HCl etch than when it is bathed in PH_3. The in situ etch also improves the mobility and decreases the background carrier concentration. Other surface studies show that a too large III/V ratio leads to hillock formation, and when the ratio is too small pits are formed.

A current and capacitance DLTS system using both voltage and optical excitation of a Schottky barrier diode has been set up to study defects at the InGaAs/InP interface. The system has been tested out, and we currently are trying to identify the traps that have been observed. This work will be continued to its completion.

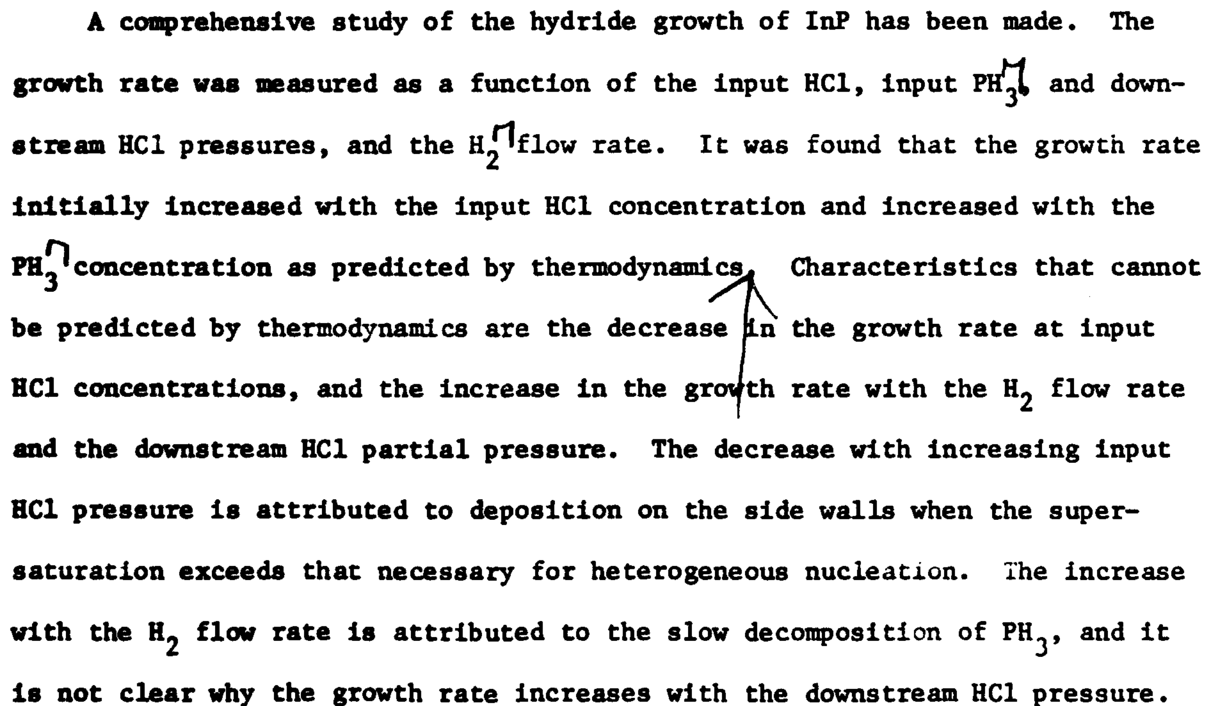

A comprehensive study of the hydride growth of InP has been made. The growth rate was measured as a function of the input HCl, input PH_3, and downstream HCl pressures, and the H_2 flow rate. It was found that the growth rate initially increased with the input HCl concentration and increased with the PH_3 concentration as predicted by thermodynamics. Characteristics that cannot be predicted by thermodynamics are the decrease in the growth rate at input HCl concentrations, and the increase in the growth rate with the H_2 flow rate and the downstream HCl partial pressure. The decrease with increasing input HCl pressure is attributed to deposition on the side walls when the supersaturation exceeds that necessary for heterogeneous nucleation. The increase with the H_2 flow rate is attributed to the slow decomposition of PH_3, and it is not clear why the growth rate increases with the downstream HCl pressure.

Using PCl_3 as a source of HCl improved the background carrier concentration of the InP buffer layers. This indicates that a primary source of the higher background carrier concentration in hydride grown films is the less pure HCl used.

I. INTRODUCTION

A. Surface and Interface Studies

The nature of the substrate surface is one of the dominant criteria that determines the characteristics of the film grown on it. Its smoothness partially determines the film smoothness; its orientation determines the film orientation, partially determines the growth rate, and strongly affects the dislocation structure; and its purity has a pronounced effect on the film purity and morphology. The nature of the substrate surface along with the type of film and the conditions under which the film is deposited determine the interface properties. The interface properties, in turn, often have a pronounced effect on device properties.

Interfacial defects can produce hysteresis in the current-voltage characteristics,[1] drift in the drain current,[2] and generate a substrate bias effect[3] in MESFET's. These effects have been attributed to the filling and emptying of deep acceptors or hole traps at the interface.[4] The small changes in the effective channel width produced by these point defects can also have a pronounced effect on the characteristics of TED's[5]. Defect states in the energy gap can increase the reverse bias tunneling current thereby increasing the response time of an InGaAs diode.[6]

For GaAs one primary defect source is chromium[4,7] from the chromium doped insulating substrate. However, other point defects are also present, and they have been attributed to transient conditions seen by the substrate surface at the beginning of growth.[7] They could, for example, be due to an anion deficiency caused by its preferential evaporation. They could also be due to surface contamination from the atmosphere such as an oxide, or contaminants introduced by the growth gases. In the case of a heterojunction, dangling bonds[8] from mismatch dislocations can also produce defect states. It is thought that cation dangling bonds produce donor bands and anion dangling bonds produce acceptor bands.[9]

Steps taken to reduce interface states include depositing a buffer layer,[10] attempting to reduce the initial growth transients by using a less abrupt start up procedure,[7] etching the substrate in situ with downstream HCl during the preheat treatment,[11,12] and finding the proper vapor composition for the growth conditions such that the composition of the solid is lattice matched to the substrate when a heteroepitaxial layer is deposited.[13]

Observing transients in the capacitance and current in the depletion region of semiconductor devices has been demonstrated to be a powerful technique for characterizing deep-level imperfection center concentrations, energy levels, thermal and optical emission rates. The original techniques developed at the University of Illinois[14] were subsequently automated at Bell Telephone Laboratories[15] to analyze exponential capacitance transients using deep-level transient spectroscopy (DLTS).

All transient techniques are based on the thermal emission of carriers from the imperfection level in a reverse biased junction. The centers can be filled with majority carriers by first zero biasing the junction. The rate of emission, e, of these carriers to the closest band edge is an exponential function of temperature given by the equation[16]

$$e = AT^2 \exp(-\Delta E/kT) .$$

Consider the simplified, but illustrative model of a Schottky barrier diode formed on an n-type material with a uniform doping level of n_d, a uniform electron trap density of n_{tn} below the conduction band, and a uniform hole trap density n_{tp} a distance E_{tp} above the valence band. Further, assume that both traps are neutral when filled; therefore, the ionized electron trap has a positive charge, and the ionized hole trap has a negative charge. As seen in figure 1a, under steady state reverse bias conditions the electron traps within a distance, x_t, of the junction

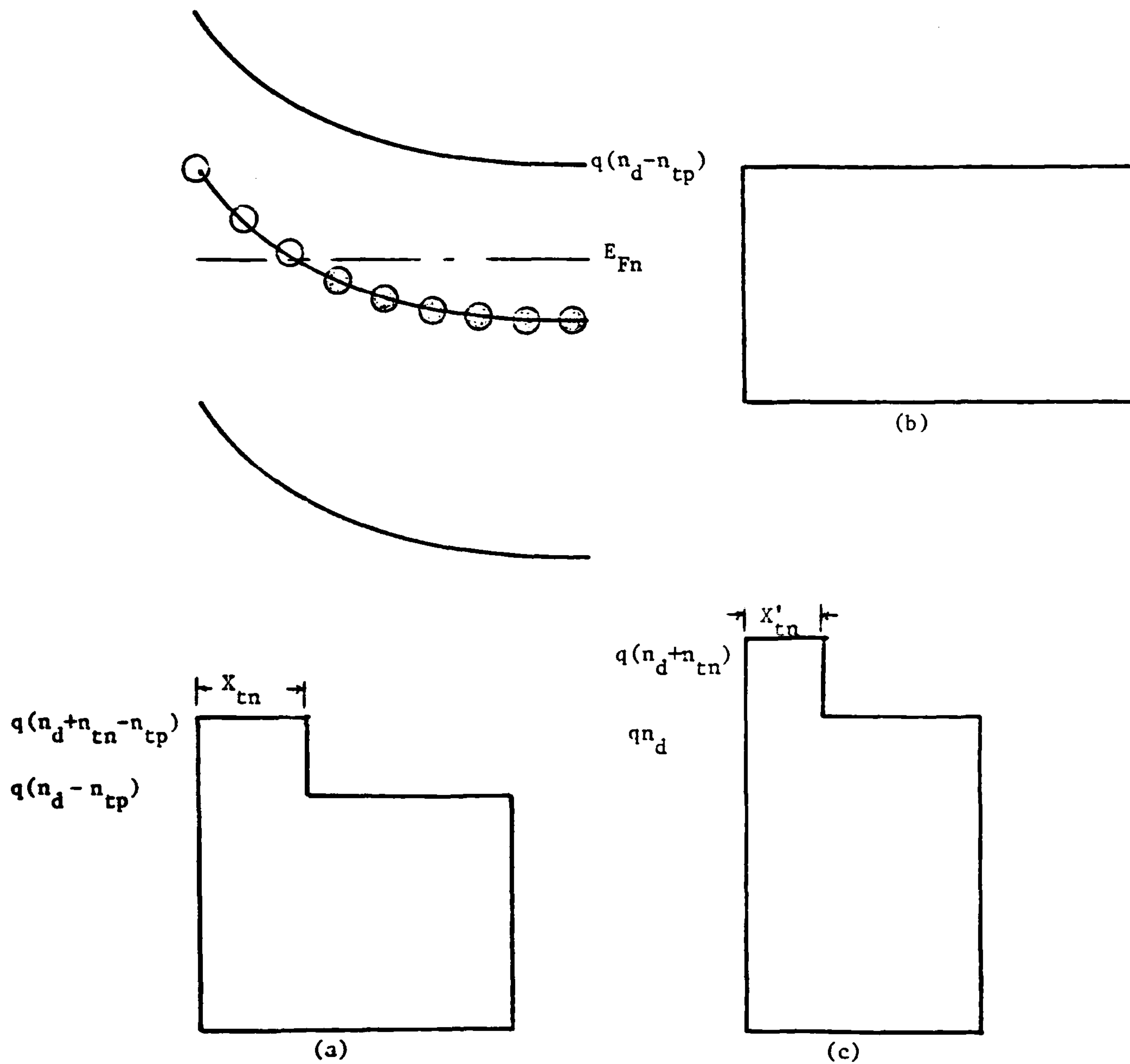

Fig. 1. a.) The band diagram and charge distribution for the steady state. b.) The charge distribution when the electron traps have been filled by a zero biasing pulse. c.) The charge distribution when the hole traps have been filled by an optical pulse.

are empty, while those in the remaining depletion layer width, $W - x_t$, are filled. x_t is determined by the point at which the energy band potential,

$$\phi = [(E_{tn} - (E_g - E_{Fn})]/q = \phi_t \quad .$$

The charge density for $0 < x < x_{tn}$ is $q\ (n_d + n_{tn} - n_{tp})$, whereas it is $q\ (n_d - n_{tp})$ for $x_t < x < W$.

When a pulse of equal, but opposite, magnitude of the reverse bias is applied, all of the traps are filled provided that the surface contact potential, $\phi_s < \phi_t$. At $t = 0$, the pulse is turned off, and the traps in the region $0 < x < x_t$ will empty over a time period, τ_{tn}. Initially, the traps are filled so the depletion region is wider in order to accommodate V_R. This is shown in figure 1b. As the traps empty, the charge near the interface increases, the depletion width narrows, and therefore the capacitance increases. Thus

$$C - C(0) = [C(\infty) - C(0)](1 - e^{-t/\tau_{tn}}).$$

The primary advantage of using optical DLTS is that it can be used to fill both minority and majority traps. The light pulse used to fill the hole traps is turned off at $t = 0$. Initially, with the traps filled the charge in the depletion layer shown in figure 1c is $q(n_d + n_{tn})$ for $0 < x < x'_{tn}$ and qn_d for $x'_{tn} < x < W$ (x'_{tn} is smaller than x_{tn} since the charge density in the depletion region is larger when the hole traps are empty). As the hole traps fill up over the entire depletion region, the charge density decreases, the depletion layer width increases, and the capacitance decreases. The capacitance is thus

$$C = C(\infty) + [C(0) - C(\infty)]e^{-t/\tau_{tp}} \quad .$$

The three parameters that are measured are the decay time, the trap depth, and the trap concentration. The time constant is obtained from $\ln\Delta C$ vs $1/T$ plots. The electron trap depth is found from the equation

$$\frac{1}{\tau_{tn}} = \sigma_{tn} v_{th} N_c \exp(-E_{tn}/kT) \quad .$$

Since $v_{th} \propto T^{1/2}$ and $N_c \propto T^{3/2}$, E_{tn} can be found from a plot of $\ln(\tau_{tn}T^2)$ vs $1/T$. For $n_t << n_d$, the trap concentration is given by

$$n_t = 2n_d \frac{|C(0) - C(\infty)|}{C(0)}$$

at the temperature for which C is a maximum.(17) There is a maximum in the $\Delta C/C$ vs T plot and the temperature is larger for deeper traps because the number of traps that empty depends on how far the electron traps are below the Fermi level. This is illustrated in figure 2. For $T << T_{max}$, $E_{tn} >> E_g - E_{F_n}$. Thus, very few of the traps empty under steady state conditions. In this simplified model none of the traps would empty if $\phi_s < [E_{tn} - (E_g - E_{Fn})]/q$. As the temperature increases, E_{Fn} decreases and when $E_g - E_{Fn}$ is only slightly less than E_{tn}, almost all of the traps will be filled at zero bias, and almost all of them will be empty under steady state conditions. This, of course, will produce a maximum in ΔC. As E_{Fn} falls further with increasing temperature, it falls below the trap level. Thus, the traps will be empty even under zero bias conditions.

When an FET structure is used, current DLTS can also be used to study traps.(18) After the traps have been filled by zero biasing, they again take time to empty. Thus, the depletion layer width of the channel and therefore the channel resistance will initially be larger. As they empty, the depletion layer and the channel resistance decrease.

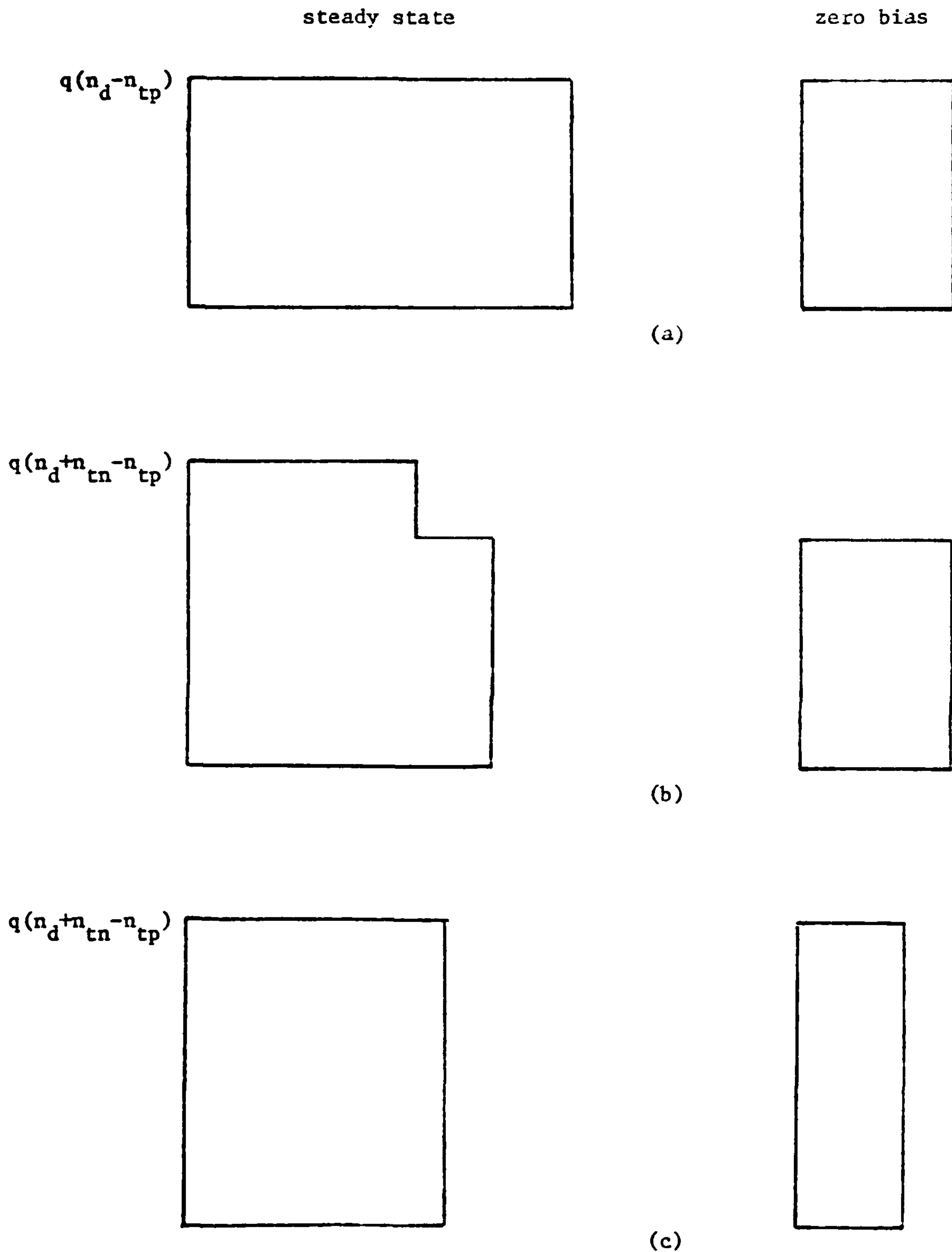

Fig. 2. a.) The steady state and zero bias charge distribution a.) at a low temperature when $E_{tn}-(E_g - E_{Fn}) > q\phi_s$, b.) when $E_g - E_{Fn}$ is almost equal to E_{tn}, and c.) when $E_g - E_{Fn} > E_{tn}$.

Studying traps at an interface can also be a method for studying interface states.[7] Interface states can be created at the substrate surface by the preferential evaporation of the anion during pregrowth[19] and the out diffusion of dopants from the substrate.[20] The former effect can to some extent be mitigated for InP by bathing it in PH_3 or AsH_3, etching it back with in situ HCl,[21] or covering the substrate.[22]

Interface states are also created by the lattice mismatch between two materials at a heterojunction. For thin films (<1 μm) the mismatch is accommodated by strain.[23] Although it is unlikely that the strain will produce a defect center, it can shift the trap energy of other centers, and it can facilitate their diffusion. For thicker films dislocations are generated to accommodate the mismatch and in addition to facilitating the diffusion of other defect centers, they, themselves, create centers. It is generally thought that dangling bonds create energy bands in the energy gap.[24-27] One can model an edge dislocation as a potential well with a long dimension parallel to the dislocation line and atomic dimensions in the two directions normal to the line.[28,29] Solutions for this model suggest there is an energy band below the middle of the gap associated with the anion dangling bonds and an energy band above the middle of the gap associated with the cation dangling bonds.

We are examining the interface states at an InGaAs/InP heterojunction using DLTS. We are initially studying the GaAs/InP heterojunction because the defect states for GaAs are well documented. Also, the heterojunction can be grown reproducibly. We plan to compare these results with those obtained for lattice matched InGaAs.

B. Growth Studies

In a previous work we did a thermodynamic analysis of the hydride growth of InP.[30] Clearly, there are both thermodynamic and kinetic effects that determine the growth characteristics. In this report we describe our experimental results on the growth of InP and discuss how they can be explained by a combination of these two effects. The primary parameter that is studied is the growth rate.

One thermodynamic prediction is that the growth rate should increase slightly superlinearly with the input HCl partial pressure, P_{HCl^o}, until the phosphorus concentration has been substantially reduced by the deposition reaction. Then the growth rate becomes sublinear. The increase with P_{HCl^o} is due to the increased InCl partial pressure which increases the supersaturation for the reaction

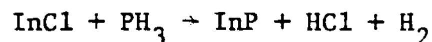

$$InCl + PH_3 \rightarrow InP + HCl + H_2$$

Erstfeld and Quinlan[31] observe a linear increase in the growth rate with P_{HCl^o}, but in the chemically similar GaAs growth system both Shaw[32] and Enstrom et al.[33] observed an initial increase in the growth rate, but it reached a maximum value and then decreased at the higher HCl^o concentrations. For growth in a chloride system, Clarke determined that the growth rate increases sublinearly with P_{HCl^o} and asymptotically approaches a maximum value.[34,35]

The supersaturation, and therefore the growth rate, increases with the input PH_3 pressure, but the increases are not as large. This is due to the fact that the chemical potential of PH_3 is less than it is for InCl. The predicted increase is less than it is for InCl. The predicted

increase is a linear increase. Erstfeld and Quinlan[31] found that the growth rate increases asymptotically with P_{PH_3}, and Shaw[32] and Enstrom et al.[33] measured a slow linear increase with P_{PH_3} for the hydride growth of GaAs.

The introduction of HCl downstream from the liquid indium boat should decrease the growth rate since it drives the reaction in the other direction. The predicted decrease is a linear decrease. This is what is observed by Erstfeld and Quinlan,[31] and by Clarke[34,35] when PCl_3 was introduced downstream. Because introducing HCl downstream decreases the supersaturation, it can prevent deposition on the side wall by keeping the saturation below that needed for heterogeneous nucleation.[12] This could lead to an increase in the growth rate since the parasitic side wall reaction could so deplete the source gases that there would be very little deposition downstream on the substrate.

Using downstream HCl could also have the beneficial effect of reducing the background carrier concentration since it decreases the activity of silicon in the quartz reactor.[36-38] Also, etching with HCl prior to deposition can greatly improve the film quality by removing surface contaminants and the indium[21,39] rich layer brought about by the preferential evaporation of phosphorus.

Finally, increasing the hydrogen flow rate while keeping the other flow rates constant should reduce the growth rate since the partial pressures, and therefore the supersaturation, are reduced. However, Zinkiewicz et al.[40] found that the growth rate increased with the H_2 flow rate. This was attributed to the slow decomposition of PH_3.[41]

Because the substrate can be a source of impurities, it is important to be able to grow a low background carrier concentration film. We attempted to do this by using PCl_3 as the source of HCl and then transporting the HCl

through an all glass system to avoid any possible contamination from stainless steel.[39]

II. EXPERIMENTAL PROCEDURE

A. Interface and Surface Studies

If an InP substrate is heated up in a hydrogen atmosphere only, phosphorus will preferentially evaporate and the surface will quickly become roughened.[19] This problem, to some extent, can be overcome by bathing the substrate in PH_3[19] or AsH_3[42] or by using a cover piece[22] during the warm up procedure. A micrograph of the substrate surface bathed in 10% PH_3 in H_2 for five minutes at a flow rate of 12.5-100 ccm is shown in figure 3a. There it is seen that small dark deposits appear on the substrate surface. The surface was scanned in an Auger-ESCA system and it was found to be very clean. It, therefore, seems likely that the spots are InP specks. In figure 3b a substrate etched in situ with .005 atm. HCl flowing at a rate of 2.5 ccm. There it is seen that this substrate surface is much smoother.

A film grown on a PH_3 treated substrate and one grown on an HCl treated substrate are shown in figure 4. In general, it is much easier to deposit a smooth film on an HCl treated surface than it is on a PH_3 treated surface.

The smoothness of the film also depends on the III/V ratio as well as the absolute partial pressures. A film grown at an HCl/PH_3 ratio of 4.0/1.5 is shown in figure 5a where it is seen that there are a number of hillocks. A film grown at an HCl/PH_3 ratio of 1.0/2.0 is shown in figure 5b where it is seen that there are a number of pits. A PH_3 heat treatment was used for both of the substrates prior to growth.

(a)

(b)

Fig. 3. Surface of an InP film bathed a.) in PH_3 with one half of the surface covered (300x) and b.) in HCl (37.5x).

Fig. 4. InP films grown on a substrate bathed in PH_3 (left) and b.) a substrate etched in HCl (right).

(a)

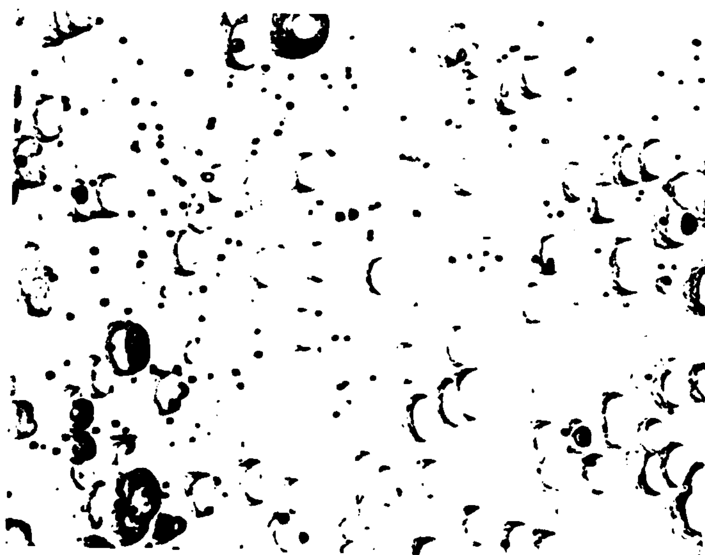

(b)

Fig. 5. InP films grown for HCl/PH_3 ratios of a.) 4.0/1.5 (37.5x) and b.) 1.0/2.0 (37.5x).

GaAs films were grown in our laboratory using the MO-CVD technique.[22] The films were then etched back to the desired thickness using a bromine-methanol etch. Ohmic source and drain contacts were made by evaporating a Au-Ge mixture through a mask, and then the contacts were annealed for 4 min. at 425°C in flowing nitrogen. Also, a 180 x 300um gold Schottky barrier was evaported on to the surface. The FET structure is illustrated in figure 6.

C-V measurements were taken using a Boonton 72B bridge with a 1 MHz signal to determine the dopant distribution. The channel resistance was measured as a function of temperature between -136°C and room temperature using a DVOM and a small drain-source voltage of $\sim$50 mV which is well within the ohmic region for the device.

For the current DLTS measurements the sample is cooled to a predetermined temperature, and a 50 mV signal at 20 kHz is applied to the system illustrated in figure 3. One current path is through R_1 and R_{ch}, while the other current path is through R_2 and the variable resistor. There is a voltage V_{AB} across R_1 that is detected by the lock in amplifier. Thus, small changes in R_{ch} can be detected as small changes in V_{AB}. The channel resistance was changed by shining pulses of 900 nm light on the junction. These measurements were performed at a series of temperatures.

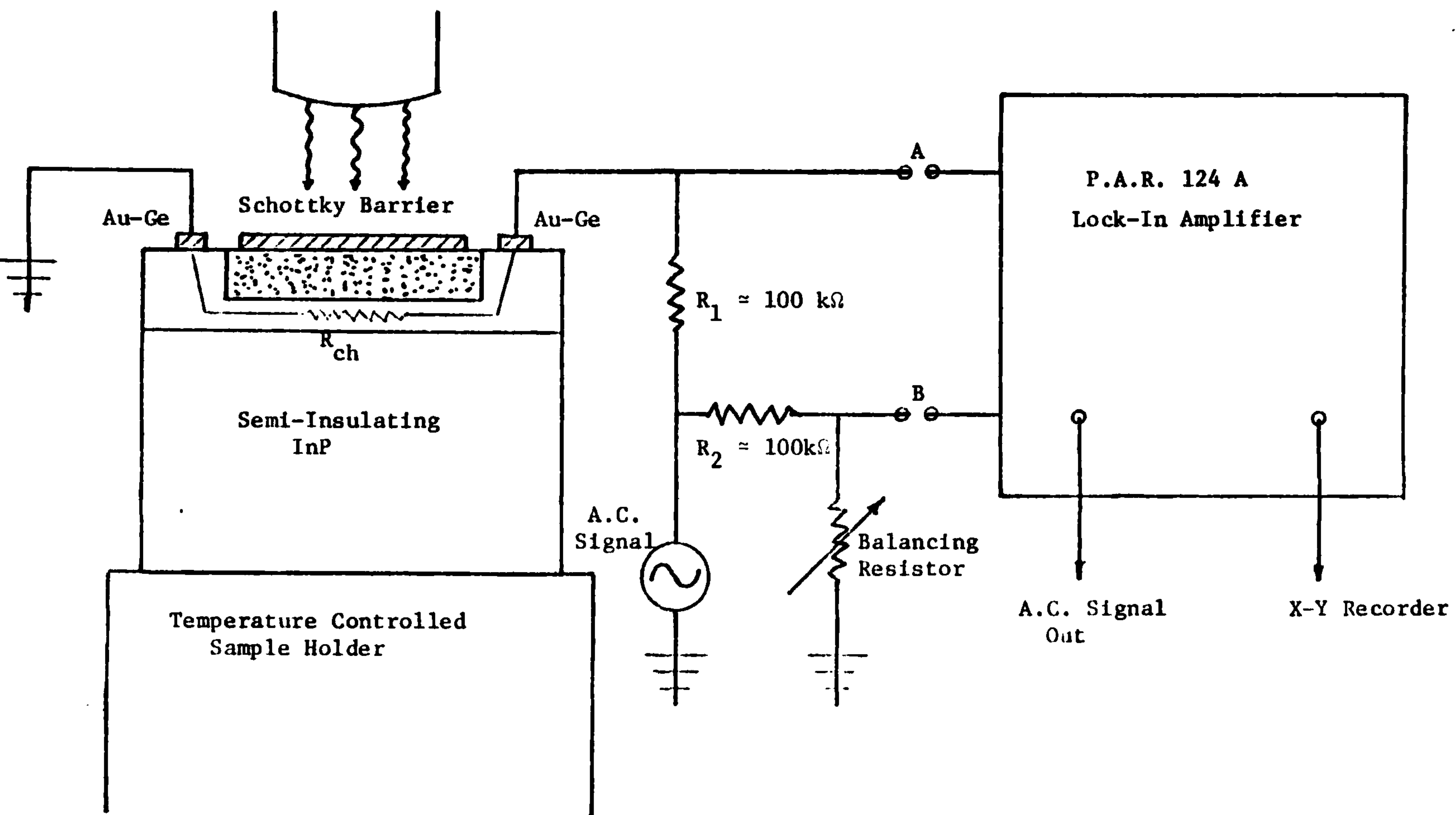

Fig. 6. The FET structure and a schematic of the electronics used in the current DLTS measurements.

A $1/C^2$ vs V curve for an etched GaAs film is shown in figure 7. The curve is linear at the smaller reverse biases, but it becomes slightly superlinear for larger values of V_R. The linear slope corresponds to a uniform doping level of 8.7×10^{14} cm^{-3}.

The channel resistance at room temperature is plotted as a function of the gate bias in figure 8. It increases linearly in the ohmic region as expected, and then begins to show signs of pinch-off at ∿2.5 V. This indicates that the interface is being approached.

The log of the channel resistance is plotted as a function of the reciprocal of the temperature in figure 9. The activation energy as indicated by the slope in the high temperature region is 57 meV whereas that in the low temperature region is 7.5 meV.

The log of the change in the channel resistance produced by the 900 nm optical pulse is plotted as a function of time for T = -136 and 26°C in figure 10. The time constant as determined from the slope of the lines are 5.1 (-136) and 1.2 (26) sec. Plots are now being made for other temperatures so that the trap energies can be determined from $T^{2}\tau$ vs 1/T plots.

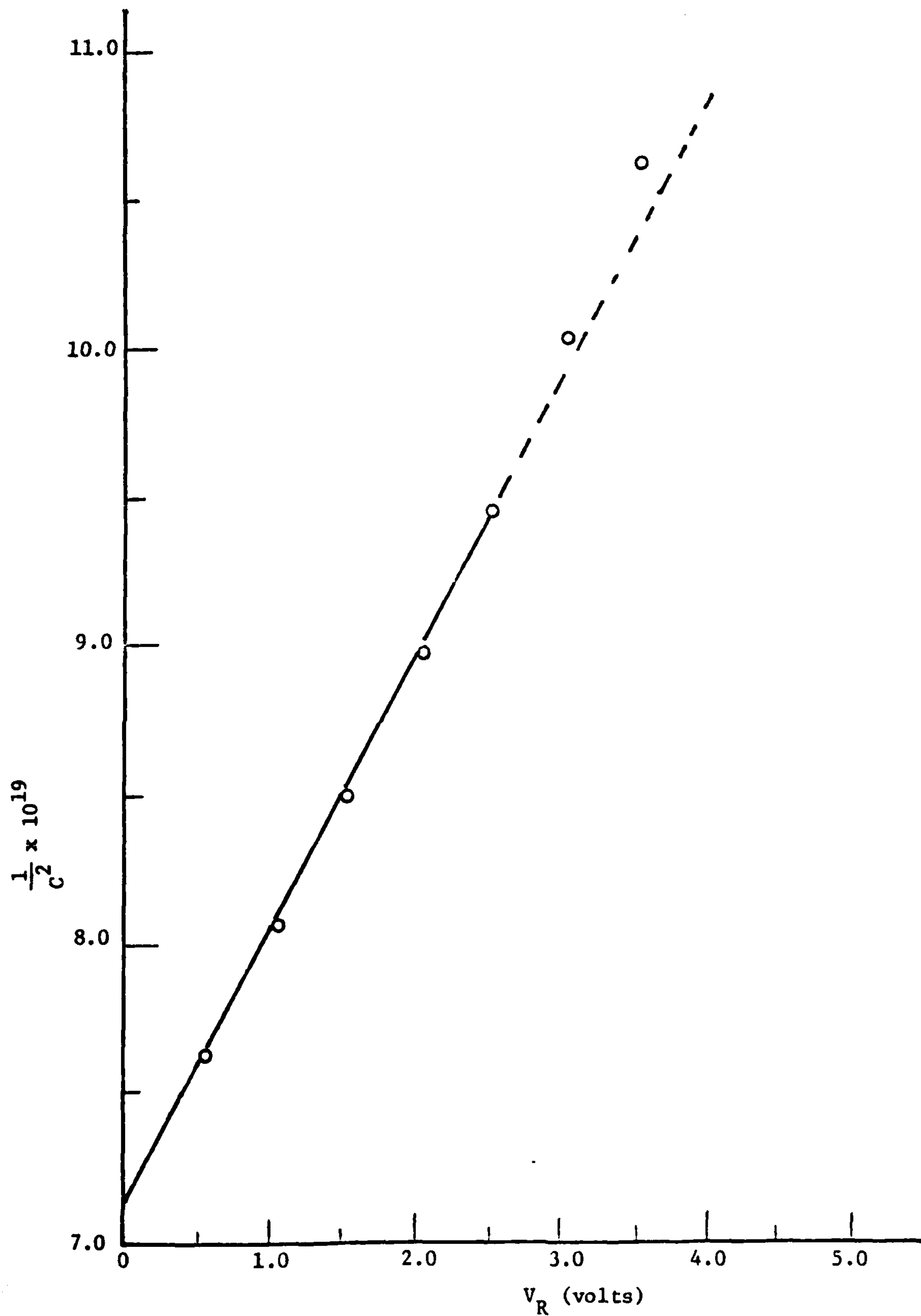

Fig. 7. The square of the reciprocal of the capacitance plotted as a function of the reverse bias for a GaAs film grown on an InP substrate.

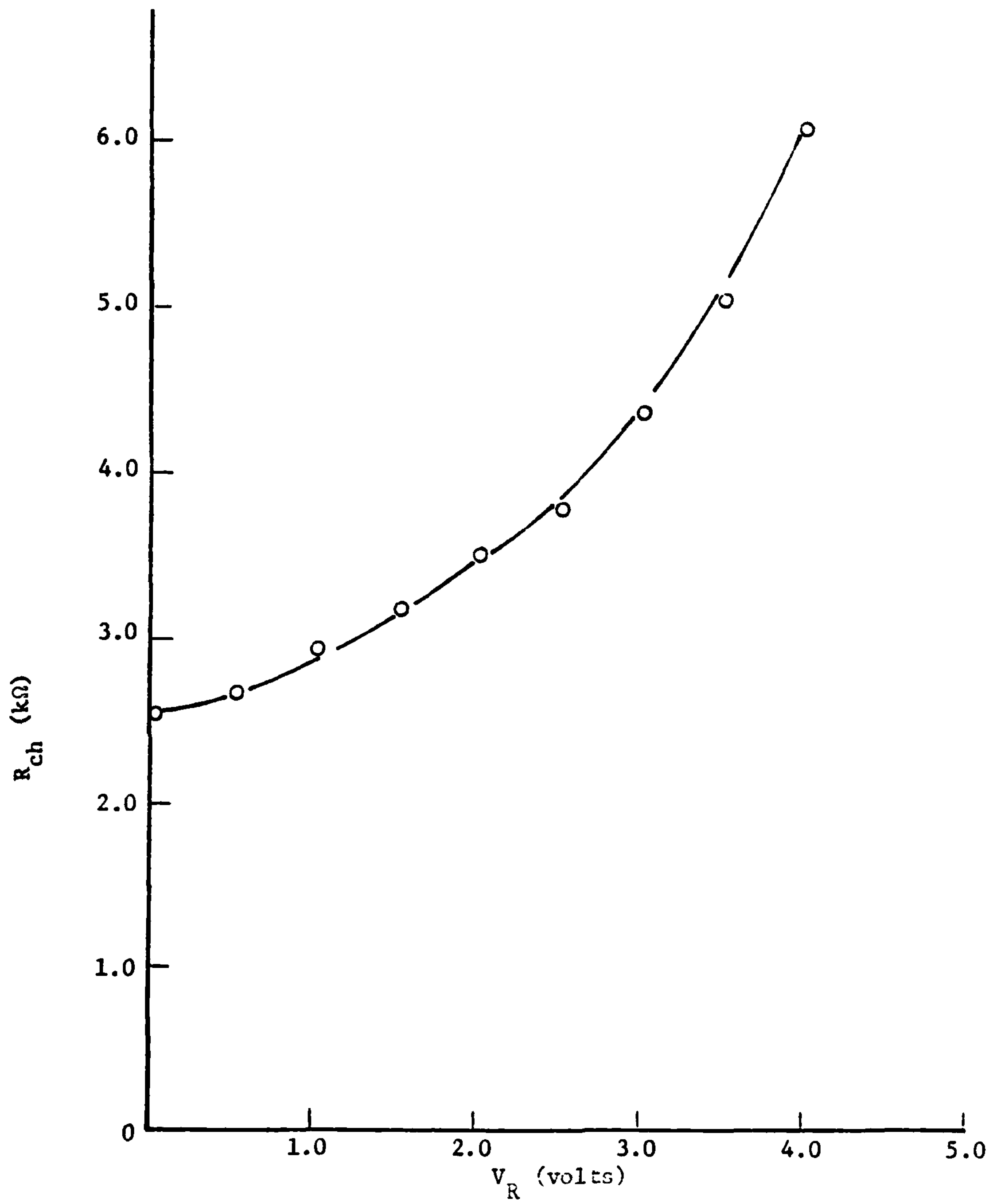

Fig. 8. The channel resistance plotted as a function of the reverse bias for a GaAs film grown on an InP substrate.

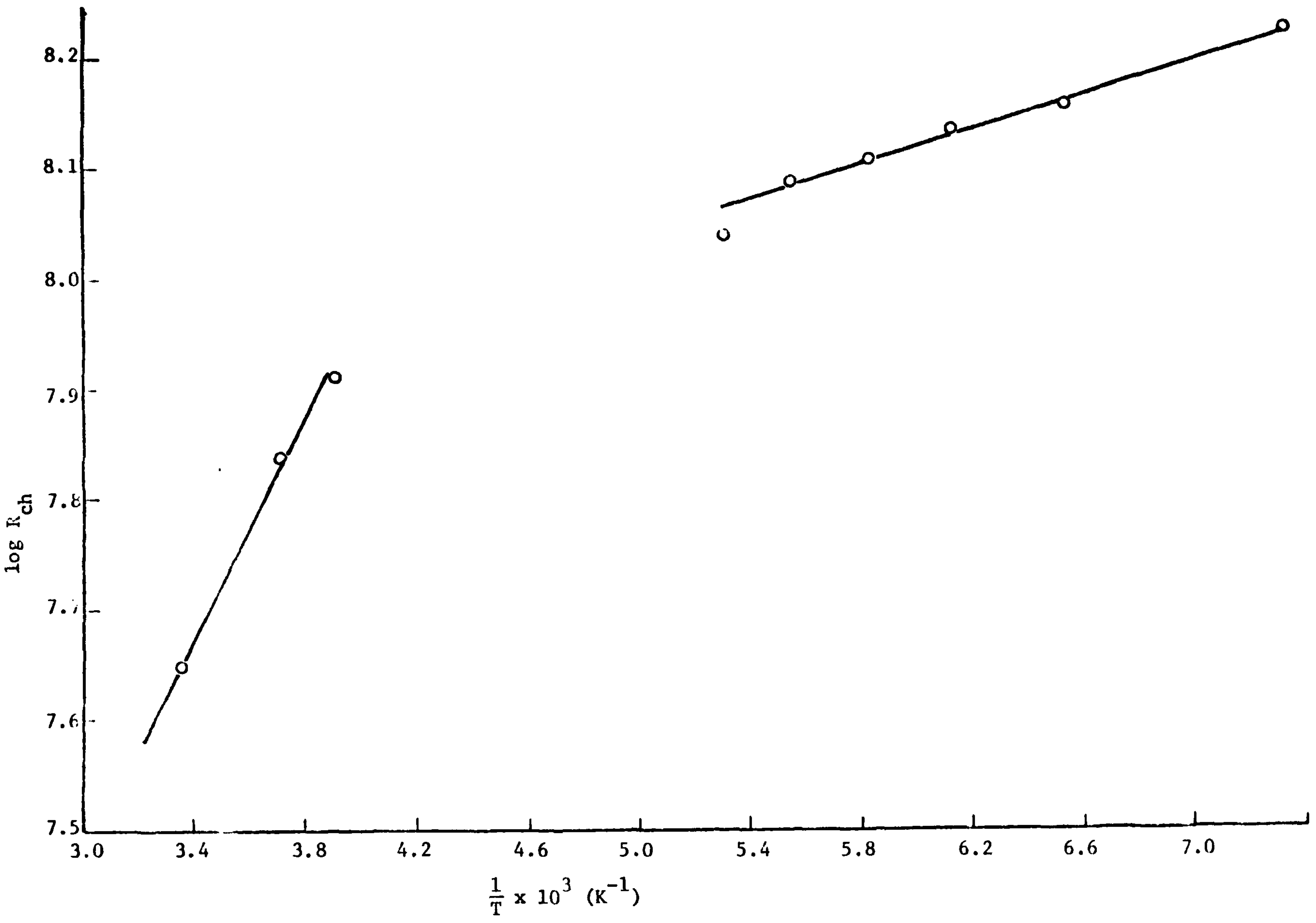

Fig. 9. The log of the channel resistance plotted as a function of the reciprocal temperature for a GaAs film grown on an InP substrate.

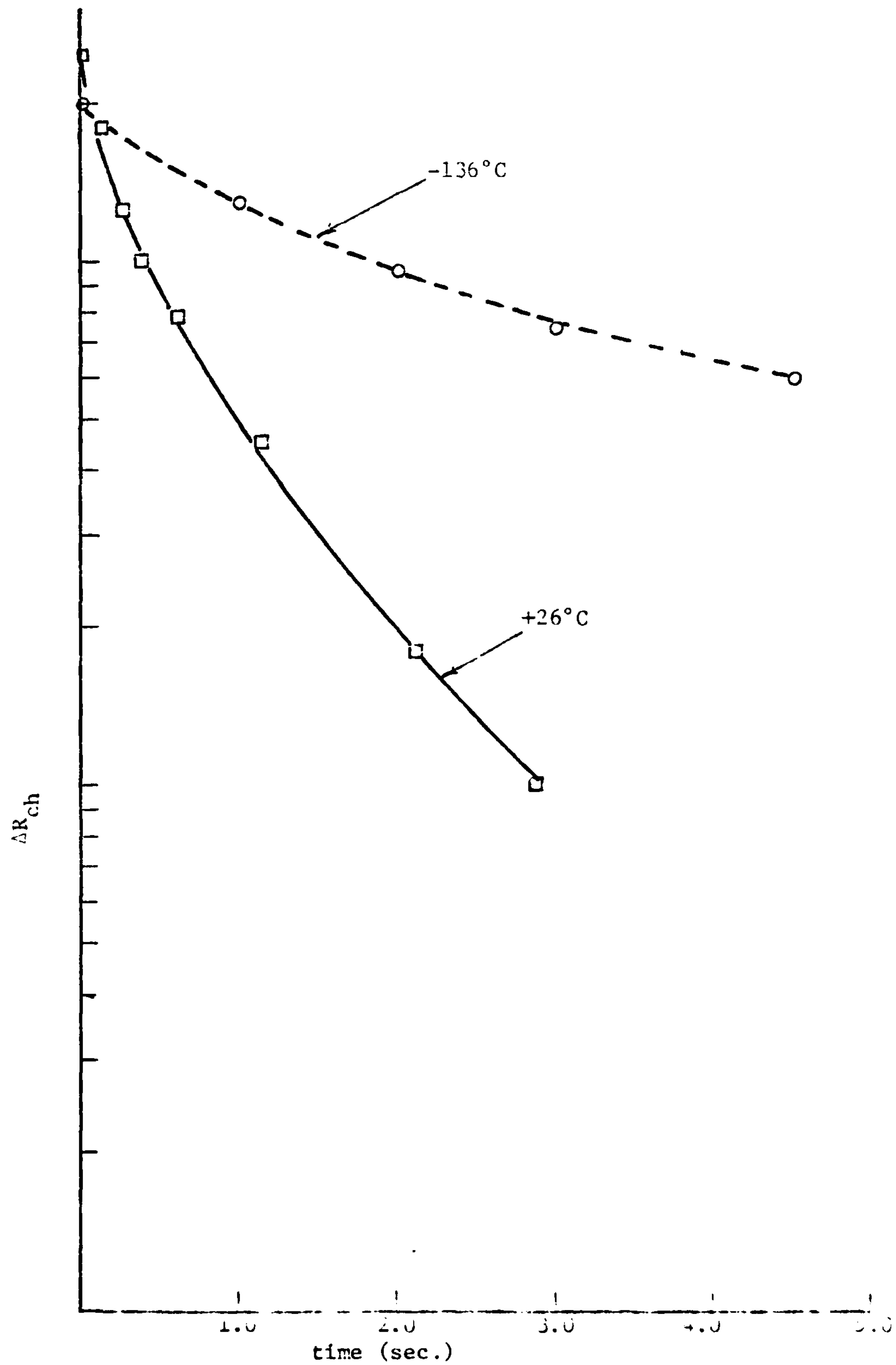

Fig. 10. The log of the change in the channel resistance plotted as a function of the time for T = -136 and 26°C for a GaAs film grown on an InP substrate.

B. Growth Studies

Six 9's pure indium was etched in a 45% KOH solution for about 30 min., and then baked in prepurified hydrogen.[43] The furnace controllers were then set to provide a flat 820°C region for the source zone and a flat 650°C region for the deposition zone, and then a polished and cleaned[43] (001) semi-insulating iron doped substrate was placed in the forechamber. The chamber was pumped down and backfilled with hydrogen several times, and then the gate valve was opened and the substrate was magnetically inserted into the predeposition zone. The deposition gases were diverted from the substrate while it was being heated up in a phosphine stream, and then the substrate was moved into the deposition position. The flow rate of the HCl and PH_3 are varied, but the total flow rate was fixed at 500 ccm. A film was grown for thirty minutes, the substrate was retracted into the forechamber closing the gate valve behind it, and the deposition gases were turned off. A downstream HCl gas flow was turned on to clean out the growth tube. The forechamber is pumped down and back filled several times, and then the film is removed.

First, the morphology is examined and then photographed using an optical microscope. Contacts are put on in a van der Pauw geometry, and the room temperature and liquid nitrogen carrier concentrations and mobilities were measured. A portion of the substrate was cleaned off, etched in on AB etch for 5 min. at 60°C,[44] and then the film thickness was measured using the optical microscope. The remaining substrate was examined and photographed in a SEM.

The growth rate is plotted as a function of the input HCl partial pressure in figures 11-13. For figure 11 there is no downstream HCl and the PH_3 input partial pressure is .01 atm., for figure 12 the PH_3 concentration has been increased to .015 atm., and for figure 13 downstream HCl has been introduced with P_{HCl^2}/P_{HCl^o} being kept constant at .1. The salient points are that the growth rate initially increases with P_{HCl^o}, (at a rate of 200 μm/min·atm.), reaches a maximum, and then decreases; increasing the PH_3 concentration and introducing HCl downstream increase the growth rate; and the position of the maximum in the growth rate is essentially the same when downstream HCl is used ($P_{HCl^o} \approx .007$ atm.), but it is at a much higher P_{HCl^o} value when more PH_3 is used ($P_{HCl^o}(max) \approx .03$).

The growth rate is plotted as a function of the PH_3 concentration in figure 14. No downstream HCl was used and $P_{HCl^o} = .007$, which is the value for the maximum in the growth rate when $P_{PH_3} = .01$ atm. The growth rate increases linearly at a rate of ~130 μm/min·atm.

The growth rate is plotted as a function of the downstream HCl concentration in figure 15. Again, $P_{HCl^o} = .007$ atm. and $P_{PH_3} = .01$ atm. Contrary to what one would predict thermodynamically, the growth rate increases with P_{HCl^2}, and it does so in a linear fashion.

The growth rate is plotted as a function of the H_2 flow rate in figure 16. The flow rates of the other gases were kept constant, and would yield partial pressures of $P_{HCl^o} = .007$ atm., $P_{PH_3} = .01$ atm., and $P_{HCl^2} =$ .0007 atm. when the hydrogen flow rate was 500 ccm. Contrary to thermodynamic predictions, the growth rate increases with the hydrogen flow rate.

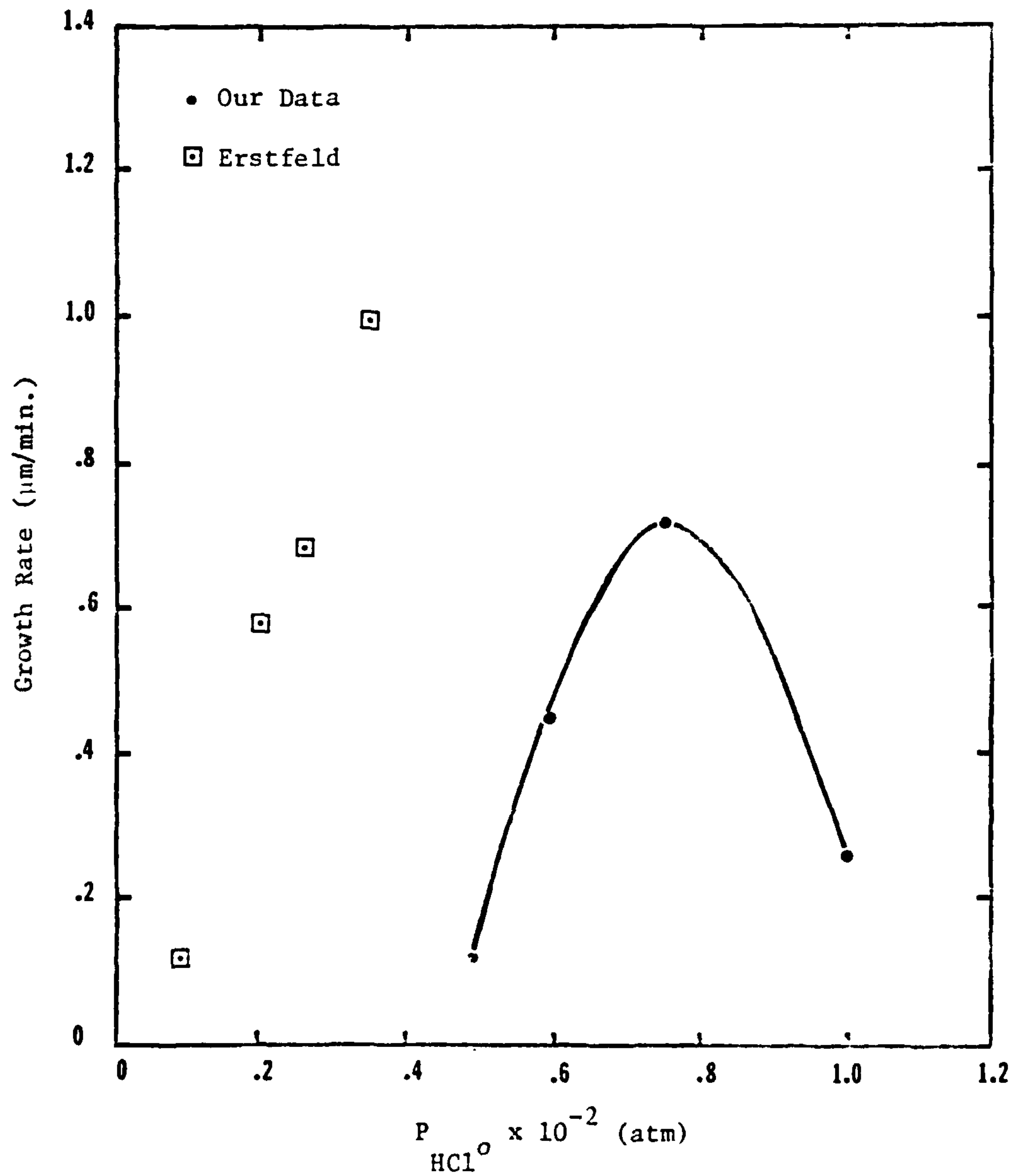

Fig. 11. The film growth rate plotted as a function of the input HCl pressure, HCl^{o}, when the partial pressures of PH_3 = .01 atm. and downstream HCl = 0.

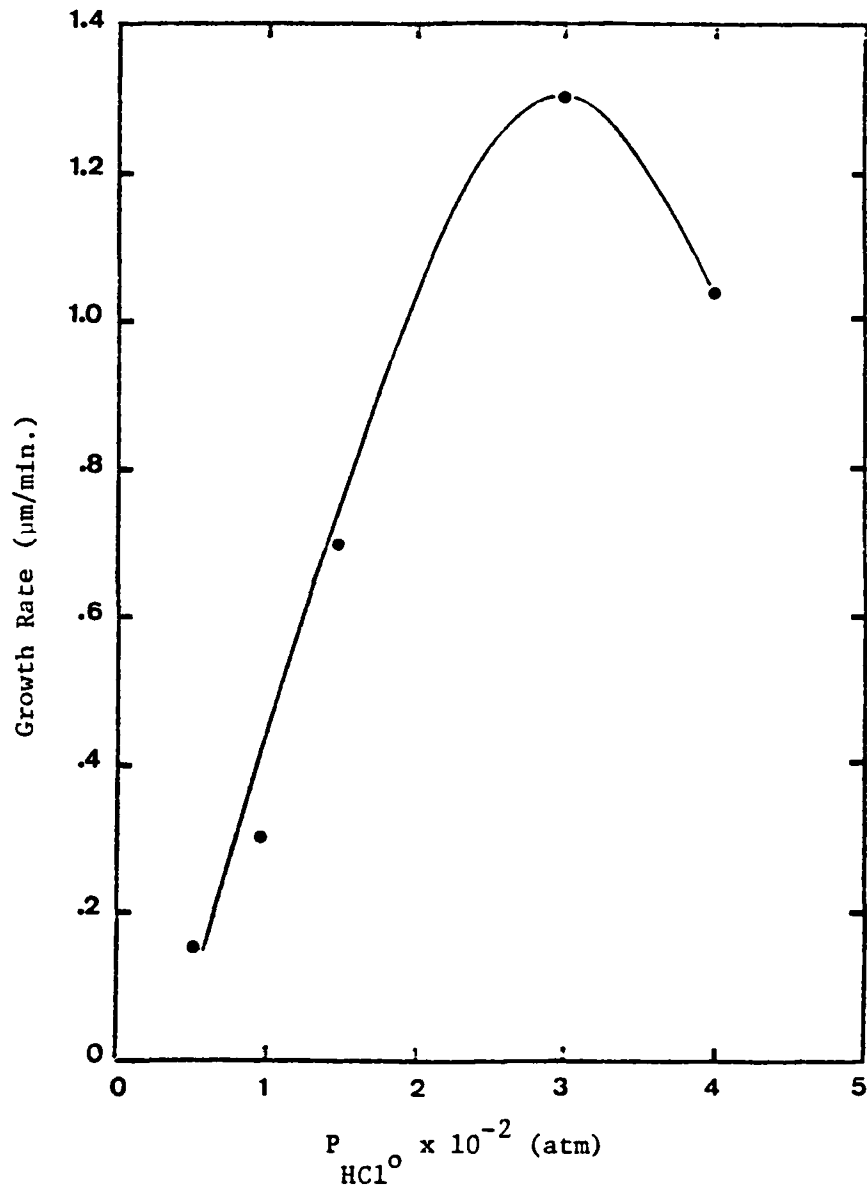

Fig. 12. The film growth rate plotted as a function of the input HCl pressure, HCl^o, when the partial pressures of PH_3 = .015 atm. and downstream HCl = 0.

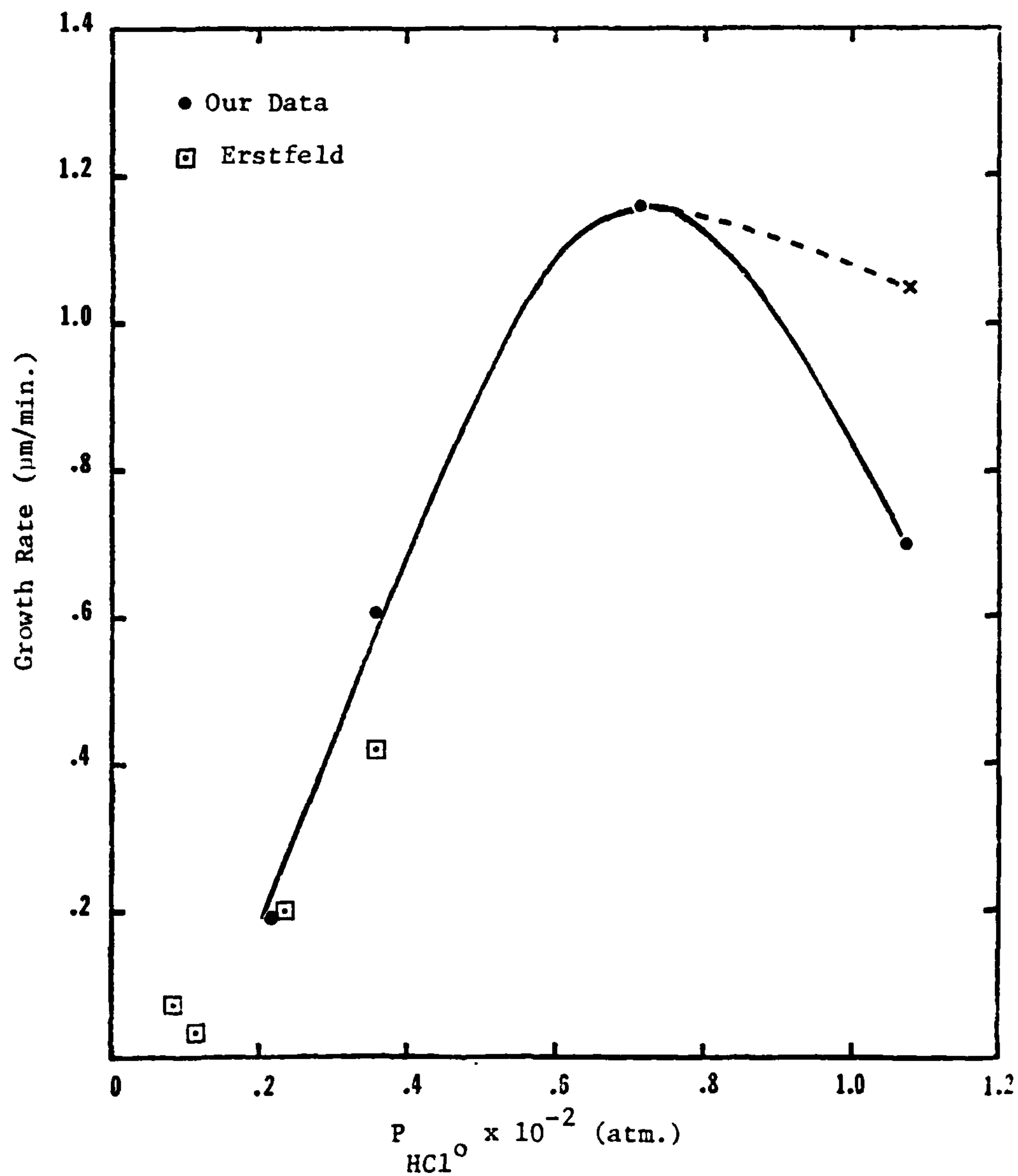

Fig. 13. The film growth rate plotted as a function of the input HCl pressure, HCl^o, when the partial pressures of PH_3 = .01 atm. and the downstream HCl = .1 P_{HCl^o}.

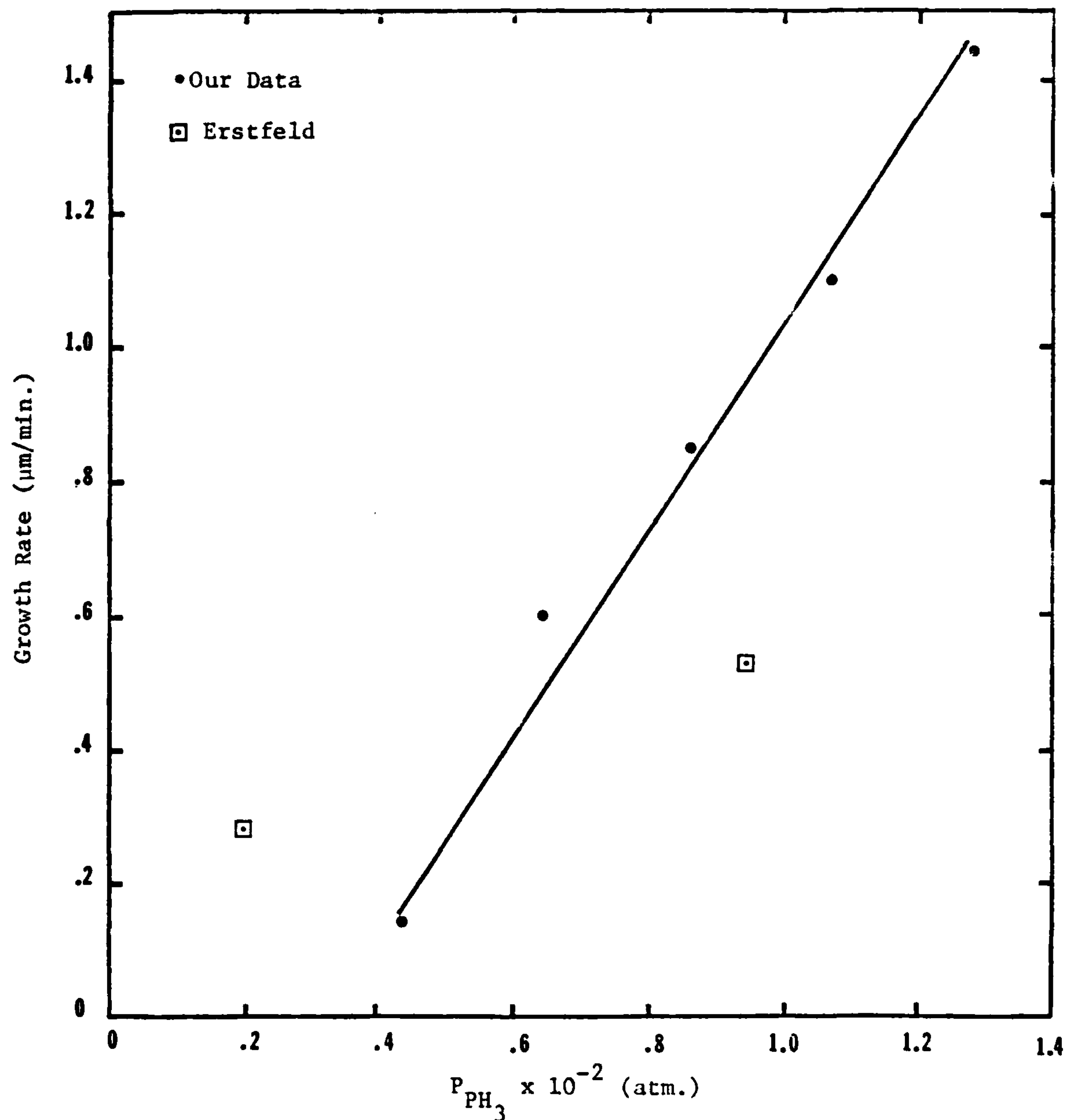

Fig. 14. The film growth rate plotted as a function of the PH_3 partial pressure when P_{HCl^o} = .007 atm. and there is no downstream HCl.

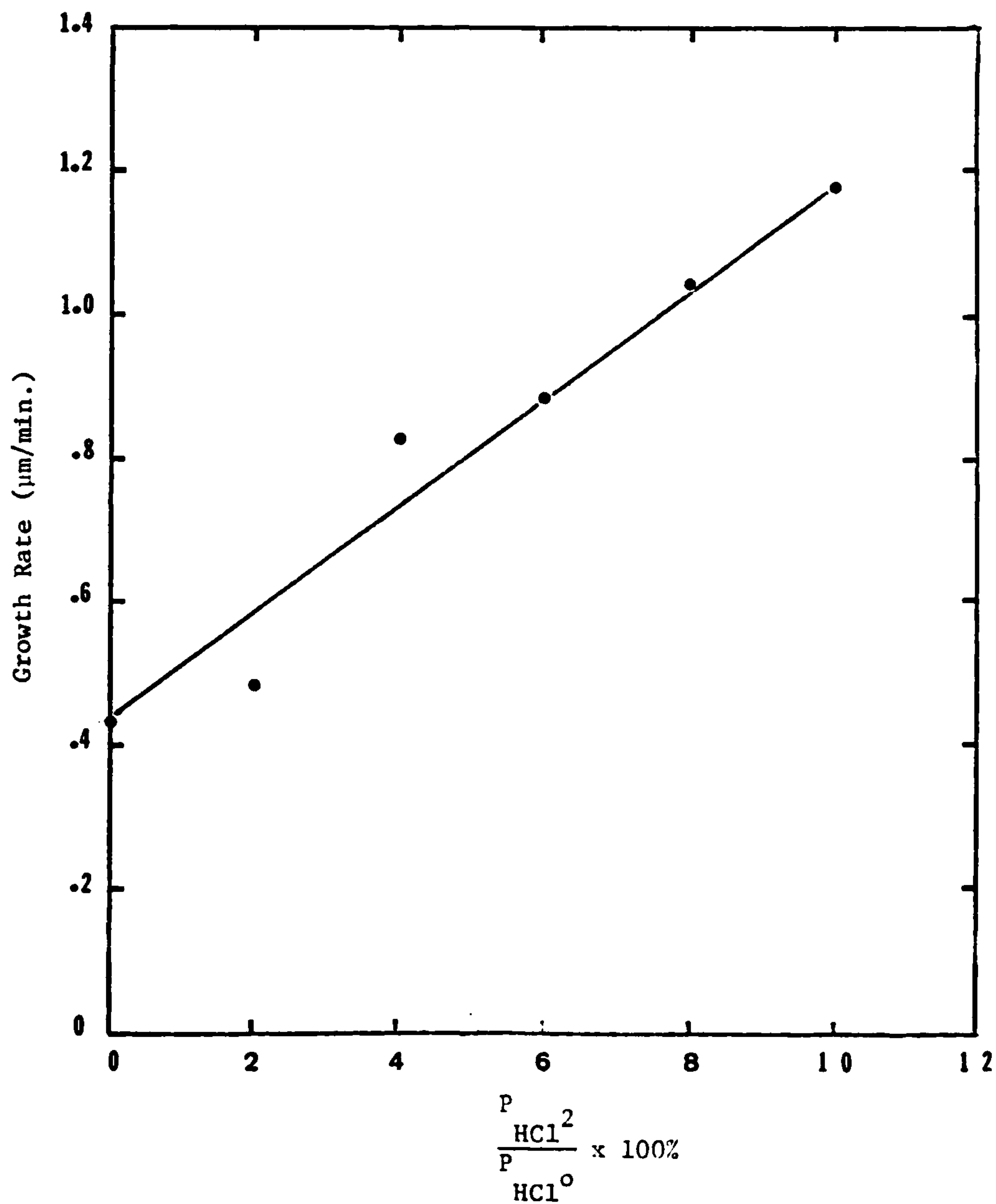

Fig. 15. The film growth rate plotted as a function of the downstream HCl pressure, P_{HCl^2}, when P_{HCl^o} = .007 atm. and P_{PH_3} = .01 atm.

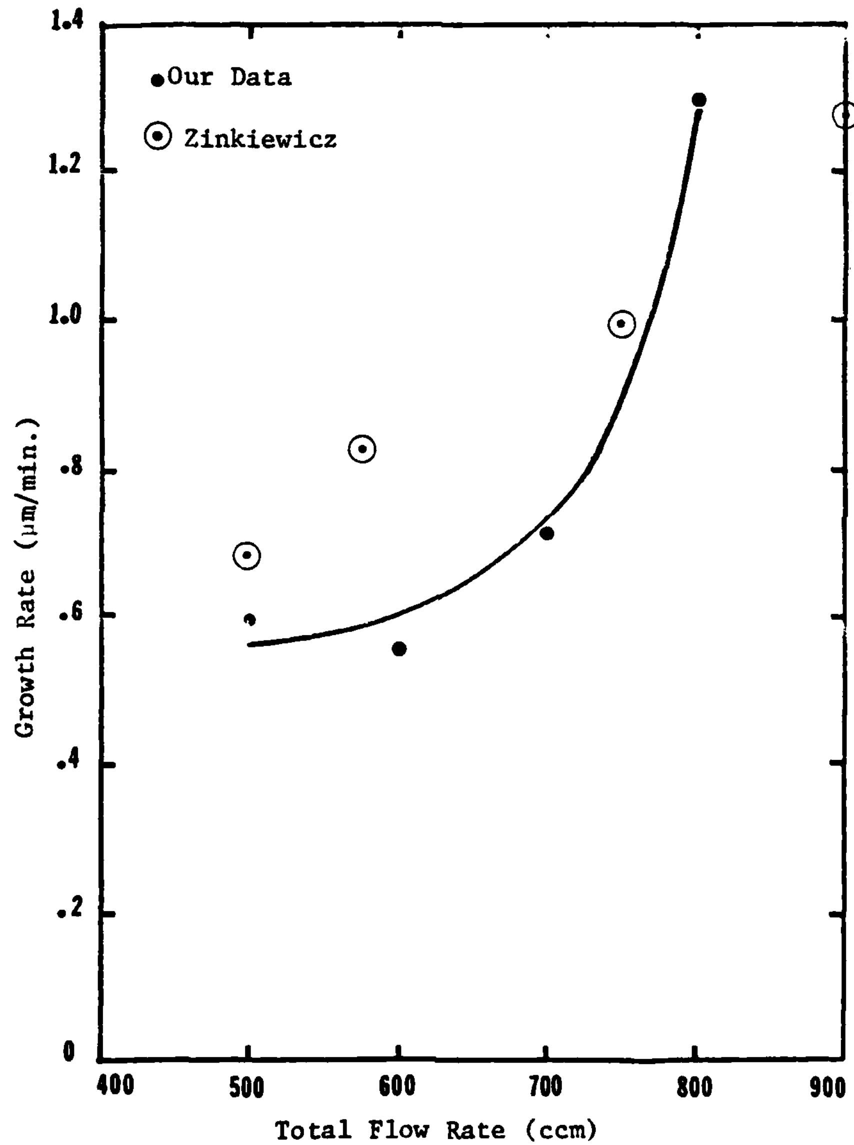

Fig. 16. The film growth rate plotted as a function of the H_2 flow rate, when the HCl^o, HCl^-, and PH_3 flow rates are held constant.

The carrier concentration and mobilities are plotted as a function of the input HCl concentration in figure 17. The lowest carrier concentration and highest mobilities were obtained when the growth rate is a maximum. Neither the carrier concentration nor the mobilities are very impressive. They were obtained using HCl from a gas cylinder instead of from the decomposition of PCl_3.

The carrier concentration and mobilities are plotted as a function of the hydrogen flow rate in figure 18. The concentrations are lower and the mobilities are higher when the flow rate, and therefore the growth rate, is higher.

An ideal buffer layer is merely an extention of the substrate without any of its impurities. Therefore, the layer should be as insulating as possible, i.e., the carrier concentration should be as low as possible. We grew films using HCl generated by cracking ultrapure (6 9's) PCl_3 in the system illustrated in figure 19. An H_2-PCl_3 mixture flows into the furnace at 900°C and the P_2 and P_4 formed by this reaction are precipitated out in the cold trap. There will be some PH_3 that is not trapped out, but thermodynamic calculations indicate that only a very small amount of phosphorus is in the PH_3 form.[45] The results shown in table 1 are very encouraging. It is seen that the background concentration in films grown from the cracked HCl is significantly smaller.

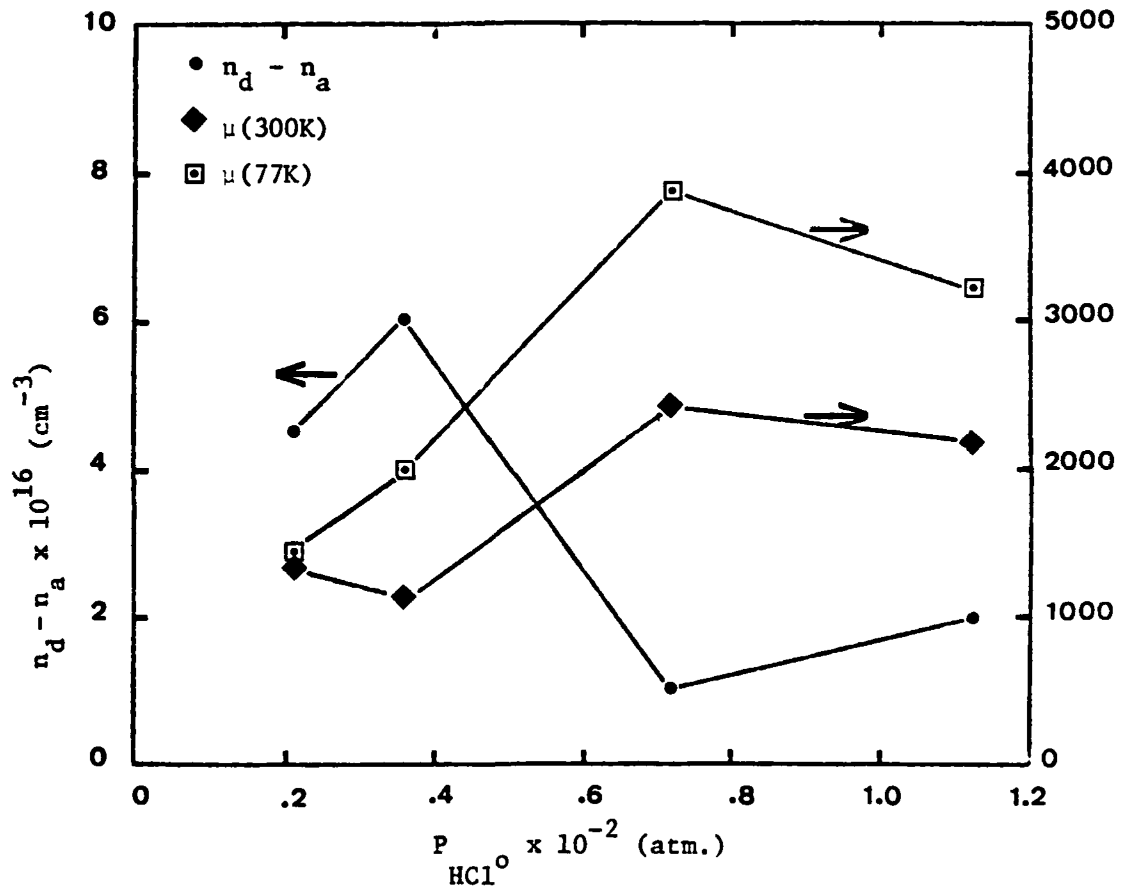

Fig. 17. The carrier concentration and the room temperature and LN mobilities plotted as a function of the input HCl concentration.

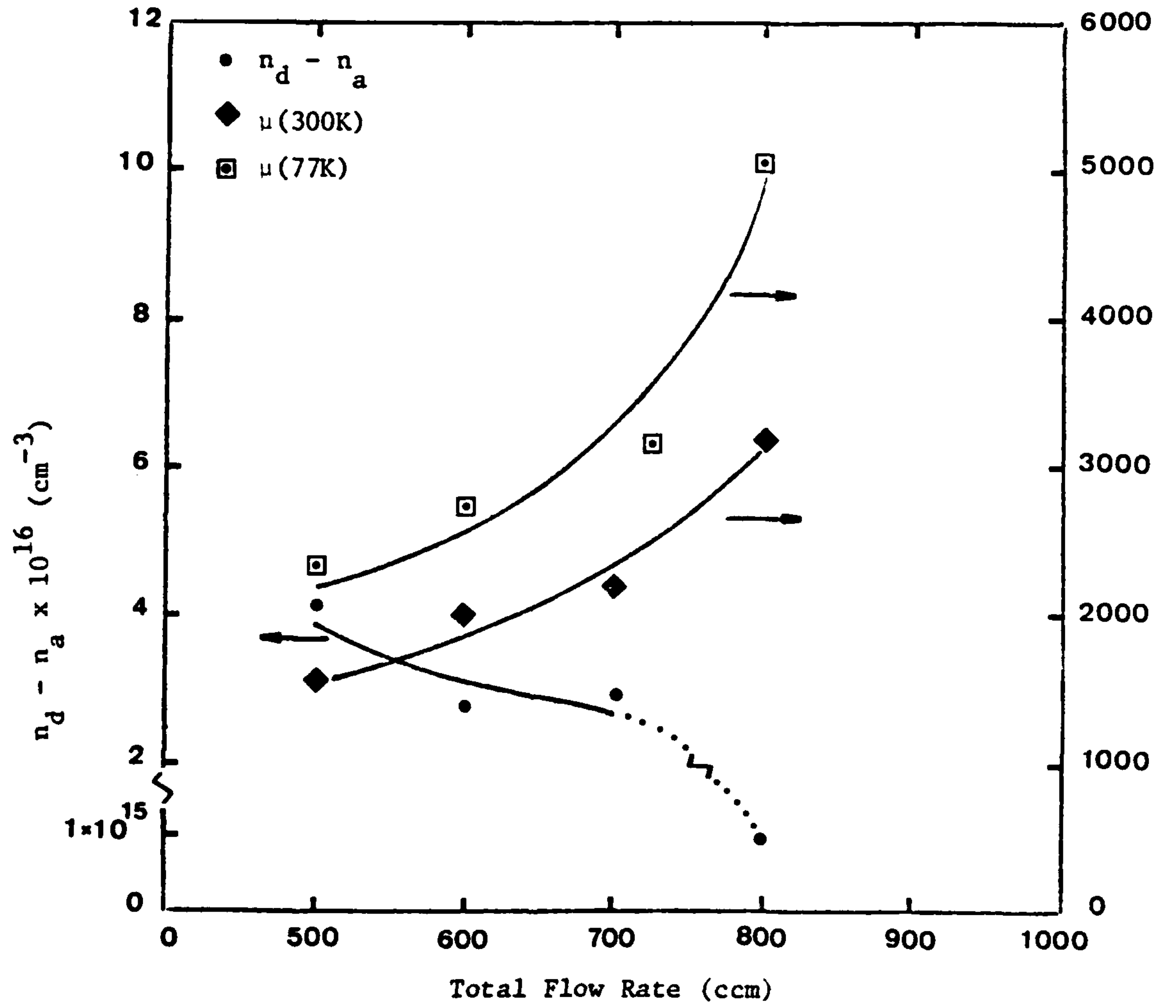

Fig. 18. The carrier concentration and the room temperature and LN mobilities plotted as a function of the H_2 flow rate.

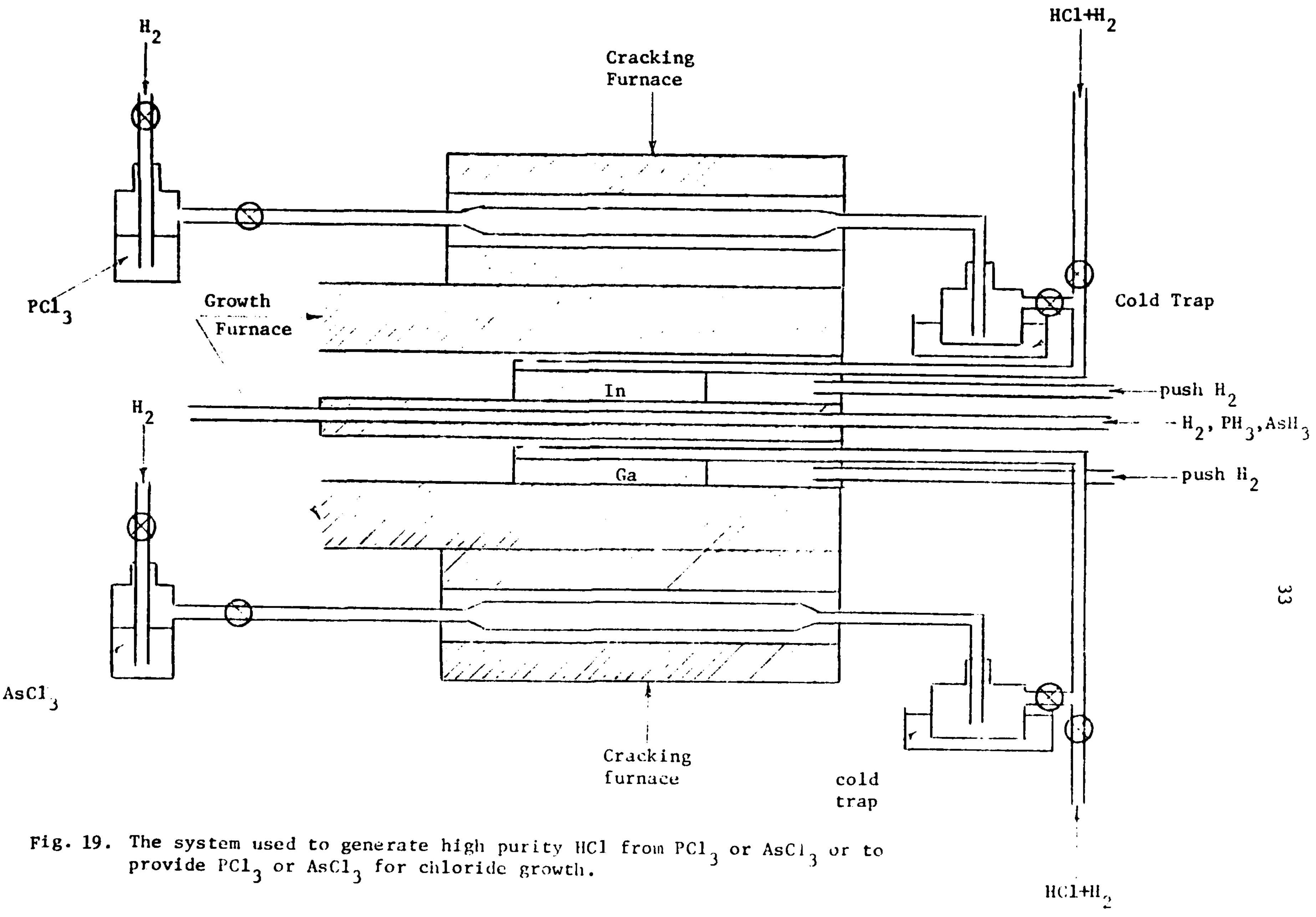

Fig. 19. The system used to generate high purity HCl from PCl_3 or $AsCl_3$ or to provide PCl_3 or $AsCl_3$ for chloride growth.

Table 1. Initial results for room temperature and 77K carrier concentrations and mobilities for HCl from a cylinder and formed by cracking PCl_3

Sample	Room Temp. Concen. cm^{-3}	Room Temp. Mobility $cm^2/V \cdot sec$	LN Temp. Concen. cm^{-3}	LN Temp. Mobility $cm^2/V \cdot sec$
1	5.1×10^{16}	1,370	4.4×10^{16}	6,750
2	8.3×10^{15}	2,560	6.0×10^{15}	15,300
3	2.7×10^{16}	1,450	1.3×10^{16}	7,600
4	1.4×10^{16}	2,140	8.8×10^{15}	11,600
1 PCl_3	6.4×10^{15}	3,300	4.4×10^{15}	25,000
2 PCl_3	7.1×10^{15}	2,700	5.7×10^{15}	20,400
3 PCl_3	3.9×10^{15}	3,930	2.2×10^{15}	28,200
4 PCl_3	4.2×10^{15}	4,100	2.9×10^{15}	29,100

We also determined that films grown on substrates subjected to an in situ etch have a lower carrier concentration. This is shown in table 2.

Table 2. Initial results for room temperature and 77K carrier concentrations and mobilities when the substrate is not etched and is etched in situ prior to deposition

Sample	Room Temp. Concen. cm^{-3}	Room Temp. Mobility $cm^2/V.sec$	LN Temp. Concen. cm^{-3}	LN Temp. Mobility $cm^2/V \cdot sec$
1	6.4×10^{15}	3,300	4.4×10^{15}	25,000
2	7.1×10^{15}	2,700	5.7×10^{15}	20,400
3	3.9×10^{15}	3,930	2.2×10^{15}	28,200
4	4.2×10^{15}	4,100	2.9×10^{15}	29,100
1 etch	3.4×10^{15}	3,600	2.7×10^{15}	28,200
2 etch	5.3×10^{15}	3,050	4.1×10^{15}	26,300
3 etch	2.7×10^{15}	4,050	2.0×10^{15}	32,100
4 etch	2.9×10^{15}	3,900	1.9×10^{15}	31,500

III. DISCUSSION

A. Interface and Surface Studies

The dark spots likely are specks of InP deposited during the preheat treatment. The phosphorus source is the PH_3 bathing it, and the indium could come from the deposits on the growth tube between the growth position and the preheat position. It seems obvious that the films grown on the HCl treated substrates are usually smoother because the substrates are usually smoother.

Others have observed during the hydride growth of GaAs[33,46] that hillocks form in a cation rich environment and pits form in an anion rich environment. The hillocks have been attributed to the formation of metal droplets formed when they do not have time to diffuse to their equilibrium position. We do not know what causes the pits to form.

The $1/C^2$ vs V_R curve indicates that the impurity incorporation is uniform except near the interface. It appears likely that the lower carrier concentration near the interface is due to the out-diffusion of iron from the semi-insulating substrate. The R_{ch} vs V_R curve indicates that the interface is approached at the larger V_R values.

The ln R vs 1/T and the $\ln \Delta R$ vs t curves illustrate that there are traps present in our GaAs film. In our continuing work we will attempt to identify these traps and determine what effect, if any, the interface has on them.

B. Growth Studies

The initial increase in the growth rate with the input HCl concentration is likely due to the increase in the supersaturation. Also, the initial increase is larger than the increase with P_{PH_3} because the chemical potential is larger. The rate of increase observed by Erstfeld and Quinlan[31] is similar.

The growth rate reaches a maximum and then decreases possibly because there is parasitic deposition on the side walls. This occurs when the

supersaturation exceeds that necessary for heterogeneous nucleation.[12] Erstfeld and Quinlan did not observe a maximum in the growth rate, but this is due to the fact that their maximum P_{HCl^o} pressures were much less than ours. Shaw[32] and Enstrom et al.[33] did observe a similar phenomenon for the hydride growth of GaAs and they attribute it to side wall deposition.

It is not clear why the maximum in the growth rate appears at a higher P_{HCl^o} value when the PH_3 pressure is increased from .01 to .015 atm. Increasing P_{PH_3} increases the supersaturation so one would expect that the critical supersaturation necessary for heterogeneous nucleation would occur at a lower input HCl partial pressure - not a higher one.

The increase in the growth rate when HCl is introduced downstream is also the opposite of what is predicted thermodynamically, and what is observed by Erstfeld and Quinlan.[31] One primary difference between our system and their's is that we use a covered boat so that the HCl is in more intimate contact with the liquid indium. As a result, our source reaction goes more nearly to completion so that the vapor will contain more InCl and less HCl under the same flow rate conditions. At very low downstream HCl pressures Mizutani and Watanabe[12] observed that the growth rate was a little higher than it was without any downstream HCl, but at higher concentrations they measured a linear decrease in the growth rate. We speculate that because we have less unreacted input HCl than the others do that our HCl concentration in the mixing zone is similar to their's when our downstream HCl flow rates are larger. It still is not clear to us why introducing even small amounts of downstream HCl should increase the growth rate.

The linear increase in the growth rate with the phosphine concentration is what one would predict from thermodynamics. A similar increase was observed by Erstfeld and Quinlan,[31] and similar observations have been made for the growth of GaAs.[32,33]

The increase in the growth rate with the H_2 flow rate is not what is expected thermodynamically. However, Zinkiewicz et al.[40] have observed this behavior, and they have speculated that it is due to the slow decomposition of PH_3.[41] It is assumed that the PH_3 more readily reacts with the InCl than does the P_2 and P_4. This interesting phenomenon should be studied further.

The carrier concentrations are lower and the mobilities are larger when the growth rates are higher. This is true whether the growth rates were increased by using the optimum input HCl pressure or whether the growth rate was increased by increasing the H_2 flow rate. It would appear that the carrier concentrations are lower because the rate of impurity incorporation does not increase as fast as the growth rate does.

We believe that lower carrier concentrations and higher mobilities in the InP films grown using HCl generated by cracking ultrapure PCl_3 is a strong indication that the higher background carrier concentration in hydride grown films when compared to chloride grown films is due to a less pure chloride source. This is supported by Abrokwah who found that low carrier concentration GaAs could be grown if the HCl purity is closely monitored.[47] Further, Enstrom and Appert[48] have recently shown that GaAs grown using HCl from a cooled (195K) cylinder has a lower carrier concentration. They attribute this to less reactivity between the HCl and the gas cylinder. We believe that not only does the HCl react with the cylinder, it also reacts with the stainless steel tubing. The sulfur found in unintentionally doped hydride grown films[49] could, in part, be due to reaction between the HCl and the stainless steel tubing.[39]

Our carrier concentrations are not quite as low and our mobilities are not quite as high as those of Zinkiewicz et al.[40] but they are comparable to those of Erstfeld and Quinlan.[31] It is encouraging to note, however, in figure 20 that for a given carrier concentration our mobilities are higher. This indicates that our films are less compensated.[50] It should be only a matter of time before we can approach the carrier concentrations and mobilities found for chloride grown films.[35,51] We believe this should be the case since we have shown that the hydride growth process is similar to the steady state chloride process.[30]

We are not sure why the films grown on substrates etched with an in situ HCl etch have a lower carrier concentration. We can only speculate that the etch removes some surface contaminants.

Fig. 20. Liquid nitrogen mobilities for InP plotted as a function of the carrier concentration.

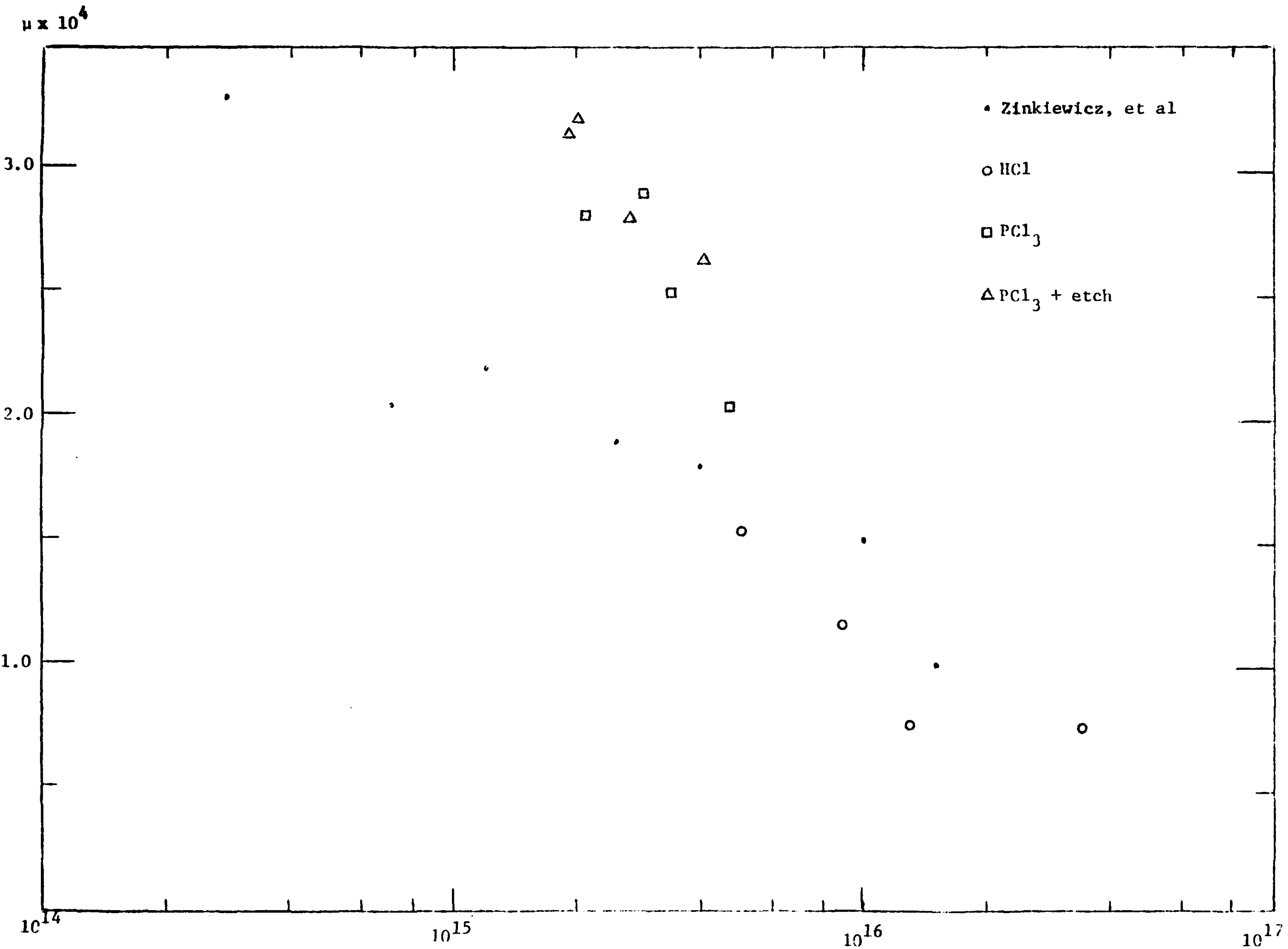

REFERENCES

1. P. L. Hower, W. W. Hooper, D. A. Tremere, W. Lehrer and C. A. Bittmann, Proc. 1968 Int. Symp. GaAs and Related Compounds, p. 187.

2. J. Barrera, Proc. 5th Bienn. Cornell Elec. Eng. Conf., Cornell Univ., Ithaca, N. Y., Aug. 1975, p. 135.

3. S. Asai, S. Ishikawa, H. Kurono, S. Takahashi and H. Kodera, Jap. J. Appl. Phys. 12, Suppl. 12-1, 71 (1973).

4. T. Itoh and H. Yanai, IEEE Trans. Elec. Dev. ED-27, 1037 (1980).

5. H. Yanai and T. Ikoma, IEEE-MTTS Int. Microwave Symp. Dig. 1976, p. 161.

6. N. Susa, Y. Yamauchi, H. Kanboe, IEEE J. Quant. Elec. QE-16, 542 (1980).

7. A Mitonneau, J. P. Chane and J. P. Andre, J. Electron. Mat., 9, 213 (1980).

8. K. A. Jones, J. Vac. Sci. Technol. 19, 578 (1981).

9. J. W. McPherson, G. Filatous, E. Stefanakos and W. Collis, J. Phys. J. Phys. Chem. Sol. 41, 747 (1980).

10. T. Nozaki, M. Ogawa, H. Terao, and H. Watanabe, Proc. 1974 Int. Symp. GaAs and Related Compounds, p. 46.

11. R. Bhat, B. J. Baliga and S. K. Ghandhi, J. Electrochem. Soc. 122, 1378 (1975).

12. T. Mizutani and H. Watanabe, J. Crystal Growth 59, 507 (1982).

13. S. B. Hyder, R. R. Saxena, S. H. Chiao and R. Yeats, Appl. Phys. Lett. 35, 787 (1979).

14. C. T. Sah, Solid State Electronics 19, 975 (1976).

15. G. L. Miller, D. V. Lang and L. C. Kimerling, Ann. Rev. Mater. Sci., 377 (1977).

16. A. S. Grove, Physics and Technology of Semiconductor Devices, (Wiley, New York, 1967) p. 131.

17. M. G. Buehler, Solid State Electronics 15, 69 (1972).

18. S. Sriram and M. B. Das, IEEE Trans. Electron Dev. 30, 586 (1983).

19. A. R. Clawson, W. Y. Lum and G. E. McWilliams, J. Crystal Growth 46, 300 (1979).

20. N. Yokoyama, A. Shibatomi, S. Ohkawa, M. Fukuta, and H. Ishikawa Proc. 1976 Int. Symp. GaAs and Related Compounds, p. 201.

21. R. Bhat and S. K. Ghandhi, J. Electrochem. Soc. 124, 1447 (1977); ibid, 125, 771 (1978).

22. C. H. Chen and K. A. Jones, to be published.

23. J. H. van der Merwe, J. Appl. Phys. 34, 117 (1963).

24. I. Alstrup and S. Markland, Phys. Status Solidi B80, 301 (1977).

25. K. D. Usadel and W. Schrater, Philos. Mag. B37, 217 (1978).

26. D. Mergel and R. Labusch, Phys. Status Solidi A42, 165 (1977).

27. M. Spencer, R. Stall, L. F. Eastman, and C. Woods, J. Appl. Phys. 50, 8006 (1979).

28. P. R. Emtage, Phys. Rev. 163, 865 (1967).

29. R. R. Holmes and C. Elbaum, Phys. Rev. 173, 803 (1968).

30. K. A. Jones, J. Crystal Growth 61, 525 (1983).

31. T. E. Erstfeld and P. Quinlan, J. Electronic Mat. 11 647, 1982.

32. D. W. Shaw, J. Electrochem. Soc. 117, 683 (1970).

33. R. E. Enstrom, C. J. Nuese, J. R. Appert and J. J. Gannon, J. Electrochem. Soc. 121, 1516 (1974).

34. R. C. Clarke and L. L. Taylor, J. Crystal Growth 43, 473 (1978).

35. R. C. Clarke, J. Crystal Growth 54, 88 (1981).

36. J. V. DiLorenzo, J. Crystal Growth 17, 189 (1972).

37. P. Rai-Choudhury, J. Crystal Growth 11, 113 (1971).

38. K. A. Jones, J. Crystal Growth 60, 313 (1982).

39. D. J. Ashen, D. A. Anderson, N. Apsley and M. T. Emeny, J. Crystal Growth 60, 225 (1982).

40. L. M. Zinkiewicz, T. J. Roth, B. J. Skromme and G. E. Stillman in: Proc. 8th Intern. Symp. on GaAs and Related Compounds Vienna, 1980 Inst. Phys. Conf. Ser. 56 (Inst. Phys. London 1981), p. 19.

41. R. H. Dalton, Proc. Roy. Soc. (London) A128, 263 (1930).

42. E. Yamaguchi, Y. Mirota, and M. Minakata, J. Crystal Growth.

43. A. R. Clawson, D. A. Collins, D. I. Elder, and J. J. Monroe, Laboratory Procedures for Etching and Polshing InP Semiconductors, N.O.S.C. Technical Note 592, (1978).

44. G. H. Olsen and M. Ettenberg, J. Appl. Phys. 45, 5112 (1974).

45. K. A. Jones, J. Crystal Growth 60, 313 (1982).

46. J. K. Kennedy and W. D. Potter, J. Crystal Growth 19, 85 (1973).

47. J. Abrokwah, T. Peck and R. Walterson, 24th Electronic Materials Conf., Ft. Collins, CO, June 1982, Paper A-3.

48. R. E. Enstrom and J. R. Appert, J. Electrochem. Soc. 129, 2567 (1982).

49. B. J. Skromme, T. S. Low, T. J. Roth, G. E. Stillman, J. K. Kennedy and J. K. Abrokwah, J. Electron. Mat. 12, 433 (1983).

50. D. L. Rode, Phys. Rev. B3, 3287 (1971).

51. K. Fairhurst, D. Lee, A. S. Robertson, H. T. Paofitt, W.H.E. Wilgoss, J. Mat. Sci. 16, 1013 (1981).

END

FILMED

02-84

DTIC